Inferring the anthropogenic NO_x emission trend over the United States during 2003 - 2017 from satellite observations: Was there a flattening of the emission trend after the Great Recession?

Jianfeng Li[1], Yuhang Wang[1*]

[1] School of Earth and Atmospheric Sciences, Georgia Institute of Technology, Atlanta, Georgia, USA

[*] *Correspondence to* Yuhang Wang (yuhang.wang@eas.gatech.edu)

Abstract

We illustrate the nonlinear relationships among anthropogenic NO_x emissions, NO_2 tropospheric vertical column densities (TVCDs), and NO_2 surface concentrations using model simulations for July 2011 over the contiguous United States (CONUS). The variations of NO_2 surface concentrations and TVCDs are generally consistent and reflect well anthropogenic NO_x emission variations for high-anthropogenic-NO_x emission regions. For low-anthropogenic-NO_x emission regions, however, nonlinearity in the emission-TVCD relationship due to emissions from lightning and soils, chemistry, and physical processes makes it difficult to use satellite observations to infer anthropogenic NO_x emission changes. The analysis is extended to 2003 – 2017. Similar variations of NO_2 surface measurements and coincident satellite NO_2 TVCDs over urban regions are in sharp contrast to the large variation differences between surface and satellite observations over rural regions. We find a continuous decrease of anthropogenic NO_x emissions after 2011 by examining surface and satellite measurements in CONUS urban regions, but the decreasing rate is lower by 9% - 46% than the pre-2011 period.

1. Introduction

Anthropogenic emissions of nitrogen oxides (NO_x = NO_2 + NO) adversely affect the environment, not only because of their direct detrimental impacts on human health (Greenberg et al., 2016; Greenberg et al., 2017; Heinrich et al., 2013; Weinmayr et al., 2009), but also their fundamental roles in the formation of ozone, acid rain, and fine particles which are unfavorable to human health, ecosystem stabilities, and climate change (Crouse et al., 2015; Kampa and Castanas, 2008; Myhre et al., 2013; Pandey et al., 2005; Singh and Agrawal, 2007). About 48.8 Tg N yr^{-1} of NO_x are emitted globally from both anthropogenic (77%) and natural (23%) sources, such as fossil fuel combustion, biomass and biofuel burning, soil bacteria, and lightning (Seinfeld and Pandis, 2016). 3.85 Tg N and 0.24 Tg N of anthropogenic and ~~natural~~ soil NO_x, respectively, were emitted from the U.S. in 2014 on the basis of the 2014 National Emission Inventory (NEI2014); vehicle sources and fuel combustions accounted for 93% of the total anthropogenic NO_x emissions (EPA, 2017).

The U.S. anthropogenic NO_x emissions during the 2010s declined dramatically compared to the mid-2000s (EPA, 2018; Xing et al., 2013) due to stricter air quality regulations and emission control technology improvements, such as the phase-in of Tier II vehicles during 2004 – 2009 and the switch of power plants from coal to natural gas (De Gouw et al., 2014; McDonald et al., 2018). The overall reduction (about 30% - 50%) of anthropogenic NO_x emissions from the mid-2000s to the 2010s was corroborated by observed decreasing of vehicle NO_x emission factors, NO_2 surface concentrations, nitrate wet deposition flux (Figure S1), and NO_2 tropospheric vertical column densities (TVCDs) (Bishop and Stedman, 2015; Georgoulias et al., 2019; Li et al., 2018; McDonald et al., 2018; Miyazaki et al., 2017; Russell et al., 2012; Tong et al., 2015). However, the detailed NO_x emission changes after the Great Recession (from December 2007 to June 2009) are highly uncertain. On the one hand, the U.S. Environmental Protection Agency

(EPA) estimated that the Great Recession had a slight impact on the anthropogenic NO_x emission trend, and the anthropogenic NO_x emissions decreased steadily from 2002 to 2017 (Figure S2~~1~~), although the emission decrease rate slowed down by about 20% after 2010 (-5.8% yr^{-1} for 2002 – 2010, and -4.7% yr^{-1} for 2010 – 2017, Table 1) (EPA, 2018). Fuel-based emission estimates in Los Angeles also showed a steady decrease of anthropogenic NO_x emissions after 2000 and a small impact of the Great Recession on anthropogenic NO_x emission decrease trend (Hassler et al., 2016). The continuous decrease of anthropogenic NO_x emissions was consistent with the ongoing reduction of vehicle emissions (McDonald et al., 2018). On the other hand, Miyazaki et al. (2017) and Jiang et al. (2018) found that the U.S. NO_x emissions derived from satellite NO_2 TVCDs, including OMI (the Ozone Monitoring Instrument), SCIAMACHY (SCanning Imaging Absorption SpectroMeter for Atmospheric CHartography), and GOME-2A (Global Ozone Monitoring Experiment – 2 onboard METOP-A), were almost flat from 2010 - 2015 and suggested that the decrease of NO_x emissions was only significant before 2010, which was completely different from the bottom-up and fuel-based emission estimates.

A complicating factor in inferring anthropogenic NO_x emission trends from the observations of NO_2 surface concentrations and satellite NO_2 TVCDs is the nonlinearity in NO_x chemistry (Gu et al., 2013; Gu et al., 2016; Lamsal et al., 2011). Although the decrease rates of both NO_2 surface concentrations and coincident OMI NO_2 TVCDs slowed down after the Great Recession over the United States, Tong et al. (2015), Lamsal et al. (2015) and Jiang et al. (2018) found that the slowdown of the decrease rates derived from NO_2 surface concentrations is 12% - 79% less than those of NO_2 TVCDs (Table 1). Secondly, the slowdown of the decrease rates of NO_2 surface concentrations and OMI TVCDs over cities and power plants (Russell et al., 2012; Tong et al., 2015) is significantly less than those over the whole contiguous United States (CONUS) (Jiang et al., 2018; Lamsal et al., 2015). Moreover, Zhang et al. (2018) found that filtering out lightning-

affected measurements could significantly improve the comparison of NO_2 surface concentration and OMI NO_2 TVCD trends over the CONUS.

In this study, we carefully investigate the relationships among anthropogenic NO_x emissions, NO_2 surface concentrations, and NO_2 TVCDs over the CONUS and evaluate the impact of the relationships on inferring anthropogenic NO_x emission changes and trends from surface and satellite observations. Section 2 describes the model and datasets used in this study, including the Regional chEmistry and trAnsport Model (REAM), the EPA Air Quality System (AQS) NO_2 surface observations, and NO_2 TVCD products from OMI, GOME-2A, GOME-2B (GOME2 onboard METOP-B), and SCIAMACHY. In Section 3, we examine the nonlinear relationships among anthropogenic NO_x emissions, NO_2 surface concentrations, and NO_2 TVCDs using model simulations. Accounting for the effects of chemical nonlinearity, we then investigate the anthropogenic NO_x emission trends and changes from 2003 – 2017 over the CONUS. Finally, section 4 gives a summary of the study.

2. Model and Data Description

2.1 REAM

The REAM model has been applied and evaluated in many research applications including ozone simulation and forecast, emission inversion and evaluations, and ~~mechanical~~ mechanistic studies of chemical and physical processes (Alkuwari et al., 2013; Cheng et al., 2017; Cheng et al., 2018; Choi et al., 2008a; Choi et al., 2008b; Gu et al., 2013; Gu et al., 2014; Koo et al., 2012; Liu et al., 2012; Liu et al., 2014; Wang et al., 2007; Yang et al., 2011; Zhang et al., 2017; Zhang et al., 2018; Zhang and Wang, 2016; Zhao and Wang, 2009; Zhao et al., 2009a; Zhao et al., 2010). REAM used in this work, the model domain of which is shown in Figure 3, has 30 vertical layers in the troposphere, and the horizontal resolution is 36 × 36 km^2. The model is driven by

meteorology fields from a Weather and Research Forecasting (WRF, version 3.6) model simulation initialized and constrained by the NCEP coupled forecast system model version 2 (CFSv2) products (Saha et al., 2011). The chemistry mechanism is based on GEOS-Chem v11.01 with updated reaction rates and aerosol uptake of isoprene nitrates (Fisher et al., 2016). Chemistry boundary conditions and initializations are from a GEOS-Chem (2° × 2.5°) simulation. Hourly anthropogenic emissions on weekdays are based on the 2011 National Emission Inventory (NEI2011), while weekend anthropogenic emissions are set to be two-thirds of the weekday emissions (Beirle et al., 2003; Choi et al., 2012). Biogenic VOC emissions are estimated using the Model of Emissions of Gases and Aerosols from Nature (MEGAN) v2.10 (Guenther et al., 2012). NO_x emissions from soils are based on the Yienger and Levy (YL) scheme (Li et al., 2019; Yienger and Levy, 1995). The cloud-to-ground (CG) lightning flashes are calculated following Choi et al. (2005) and Zhao et al. (2009a) with the parameterization of CG flash rate as a function of convective mass fluxes and convective available potential energy (CAPE). The ratios of intra-cloud (IC) lightning flashes to CG flashes are parameterized as a function of the height between the freezing layer and the cloud top (Luo et al., 2017; Price and Rind, 1992). In this study, 250 moles of NO are emitted per CG or IC flash (Zhao et al., 2009a). As a result, on weekdays in July 2011, REAM has mean anthropogenic NO_x emissions of 7.4×10^{10} molecules cm^{-2} s^{-1}, mean soil NO_x emissions of 1.2×10^{10} molecules cm^{-2} s^{-1}, and mean lightning NO_x emissions of 3.4×10^{10} molecules cm^{-2} s^{-1} over the CONUS.

2.2 Satellite NO_2 TVCDs

In this study, we use NO_2 TVCD products from four satellite ~~measurements~~ sensors in the past decade, including SCIAMACHY, GOME-2A, GOME-2B, and OMI, the spectrometers onboard sun-synchronous satellites to monitor atmospheric trace gases. The SCIAMACHY instrument onboard the Environmental Satellite (ENVISAT) has an equator overpass time of 10:00 Local time (LT) and a nadir pixel resolution of 60 × 30 km^2. The GOME-2 instruments on

Metop-A (named as GOME-2A) and Metop-B (GOME-2B) satellites cross the equator at 9:30 LT and have a nadir resolution of 80 × 40 km^2. After July 15, 2013, the nadir resolution of GOME-2A became 40 × 40 km^2 with a smaller scanning swath. The OMI onboard the EOS-Aura satellite has a nadir resolution of 24 × 13 km^2 and overpasses the equator around 13:45 LT. More detailed information about these instruments is summarized in Table S1. These instruments measure ~~transmitted,~~ backscattered~~, and reflected~~ solar radiation from the atmosphere in the ultraviolet and visible wavelength. The radiation measurements in the wavelength of 402 - 465 nm are then used to retrieve NO_2 VCDs. The retrieval process consists of three steps: 1) converting radiation observations to NO_2 slant column densities (SCDs) by using the Differential Optical Absorption Spectroscopy (DOAS) spectral fitting method; 2) separating tropospheric SCDs and stratospheric SCDs from the total NO_2 SCDs; 3) dividing the NO_2 tropospheric SCDs by the tropospheric air mass factors (AMF) to compute VCDs.

The product archives we use in this study include GOME-2B (TM4NO2A v2.3), SCIAMACHY (QA4ECV v1.1), GOME-2A (QA4ECV v1.1), OMI (QA4ECV v1.1, hereafter referred to as OMI-QA4ECV), OMNO2 (SPv3, hereafter referred to as OMI-NASA), and the Berkeley High-Resolution NO_2 products (v3.0B, hereafter referred to as OMI-BEHR). OMI-BEHR uses the tropospheric SCDs from OMI-NASA products but updates some inputs for the tropospheric AMF calculation (Laughner et al., 2018). These product archives have been previously validated (Boersma et al., 2018; Drosoglou et al., 2017; Drosoglou et al., 2018; Krotkov et al., 2017; Laughner et al., 2018; Wang et al., 2017; Zara et al., 2018). Generally, the pixel-size uncertainties of these products are > 30% over polluted regions under clear-sky conditions. We summarize the basic information about these products in Table S2. To keep the high quality and sampling consistency of NO_2 TVCD datasets, we chose pixel-size NO_2 TVCD data using the criteria listed in Table S3. After the selection, we re-gridded the pixel-size data into the REAM 36 × 36 km^2 grid cells and calculate the seasonal means of each grid cell with

corresponding daily values on weekdays (winter: January, February, and December; spring: March, April, and May; summer: June, July, and Autumn; autumn: September, October, and November). We excluded weekend data in this study to minimize the impacts of weekend NO_x emission reduction, leading to different NO_2 TVCDs between weekdays and weekends (Figure S3~~2~~).

Satellite TVCD measurements can show large variations and apparent discontinuities due in part to the effects of cloud, lightning NO_x, the shift of satellite pixel coverage, and retrieval uncertainties (Figure S3~~2~~; e.g., (Boersma et al., 2018; Zhang et al., 2018)). However, continuous and consistent measurements are required for reliable trend analyses. In addition to the criteria of data selection in Table S3, we compute the seasonal relative 90th percentile confidence interval, defined as RCI = (X(95th percentile) - X(5th percentile)) / mean(X), where X is the daily NO_2 TVCD for a given season. To compute the seasonal trend, we require that RCI is < 50% for the selected season every year in the analysis period (Table S3). About 45% of data are removed as a result.

2.3 Surface NO_2 measurements

Hourly surface NO_2 measurements from 2003 - 2017 are from the EPA AQS monitoring network (archived on https://www.epa.gov/outdoor-air-quality-data). Most AQS monitoring sites use the Federal Reference Method (FRM) — gas-phase chemiluminescence to measure NO_2. Few sites use the Federal Equivalent Method (FEM) – photolytic-chemiluminescence or the Cavity Attenuated Phase Shift Spectroscopy (CAPS) method. FRM and FEM are indirect methods, in which NO_2 is first converted to NO and then NO is measured through chemiluminescence measurement of NO_2* produced by NO + O_3. The difference is that FRM uses heated reducers/catalysts for the conversion of NO_2 to NO and FEM uses photolysis of NO_2 to NO. The conversion to NO in the FRM instruments is not specific to NO_2, and non-NO_x active nitrogen

compounds (NO_z) can also be reduced by the catalysts, which would cause high biases of NO_2 measurements, while the FEM method is sensitive to the photolysis conversion efficiency of NO_2 to NO (Beaver et al., 2012; Beaver et al., 2013; Lamsal et al., 2015). The CAPS method directly determines NO_2 concentrations based on a NO_2-induced phase shift measured by a photodetector. The CAPS instrument operates at a wavelength of about 450 nm and may overestimate NO_2 concentrations due to absorption of other molecules at the same wavelength (Beaver et al., 2012; Beaver et al., 2013; Kebabian et al., 2005).

Due to the different characteristics of the above three methods and demonstrated biases between the FRM and the FEM by Lamsal et al. (2015), we firstly investigate the measurement discrepancies among the above three methods. There are three sites having FRM and FEM measurements simultaneously during some periods from 2013 - 2014, two sites having both FRM and CAPS data during some periods from 2015 – 2016, and one site using all three measurement methods during some periods in 2015. Figure S4~~3~~ shows the hourly averaged ratios of FEM and CAPS to FRM data, respectively, for 4 seasons during 2013 – 2016. The CAPS/FRM ratios are in the range of 0.94 – 1.06 and the FEM/FRM ratios of 0.86 – 1.11. Furthermore, Zhang et al. (2018) discussed that the relative trends are not affected by scaling the observation data. As in the work by Zhang et al. (2018), we analyze the relative trends in the surface NO_2 data. We, therefore, did not scale the FRM data. At sites with FEM or CAPS measurements, we use these measurements in place of FRM data. If both FEM and CAPS data are available, we use the averages of the two datasets.

Since NO_2 surface concentrations have significant diurnal variations (Figure S5~~4~~), we choose the data at 9:00-10:00 LT for comparison with GOME-2A/2B data, 10:00-11:00 LT for comparison with SCIAMACHY data, and 13:00-14:00 LT for OMI data. The seasonal *RCI* < 50% requirement is also used here to be consistent with the analysis of satellite TVCD data, and thus about 1.5% of the data are removed. We also require that the measurement site must have

196 valid measurements in the aforementioned 3 hours for at least one season from 2003 – 2017. The
197 locations of the 179 selected sites using the site selection criteria are shown in Figure 1. The
198 region definitions follow the U.S. Census Bureau (https://www2.census.gov/geo/pdfs/maps-
199 data/maps/reference/us_regdiv.pdf).

200 3. Results and Discussions

201 3.1 Nonlinear relationships among anthropogenic NO_x emissions, NO_2 surface
202 concentrations, and NO_2 TVCDs

203 NO_2 surface concentrations and NO_2 TVCD are not linearly correlated with NO_x emissions
204 due in part to chemical nonlinearity, wet and dry depositions, transport effects, background
205 sources (Gu et al., 2013; Lamsal et al., 2011). Therefore, it is necessary to first investigate the
206 nonlinearities among NO_x emissions, NO_2 surface concentrations, and TVCDs over the CONUS
207 before we compare the trends between NO_2 surface concentrations and TVCDs. The nonlinearity
208 between NO_x emission and NO_2 TVCD is analyzed by examining the local sensitivity of NO_2
209 TVCD to NO_x emissions (Gu et al., 2013; Lamsal et al., 2011; Tong et al., 2015), which is
210 defined as β in Equation (1). We further define γ as the sensitivity of NO_2 surface concentration
211 to NO_x emission:

212 $$\frac{\Delta E}{E} = \beta \frac{\Delta \Omega}{\Omega} \quad (1)$$

213 $$\frac{\Delta E}{E} = \gamma \frac{\Delta c}{c} \quad (2)$$

214 where E denotes NO_x emission and ΔE denotes the change of NO_x emission; Ω denotes NO_2
215 TVCD, c denotes surface NO_2 concentration, and $\Delta\Omega$ and Δc denote the corresponding changes.

We computed β and γ values for July 2011 over the CONUS using REAM. To compute local β and γ values, we added another independent group of chemistry species ("group 2") in REAM in order to compute the standard and sensitivity simulations concurrently. The original chemical species in the model ("group 1") were used in the standard simulation. For group 2 chemical species, anthropogenic NO_x emissions were reduced by 15%. In the model simulation, we first computed the advection of group 1 tracers. The horizontal tracer fluxes were therefore available. All influxes into a grid cell for group 2 tracer simulation were from group 1 tracer simulation; only outfluxes were computed using group 2 tracers. The outflux was one way in that nitrogen species were transported out but the transport did not affect adjacent grid cells because the influxes were from group 1 tracer simulation. Using this procedure, the effects of anthropogenic NO_x emission reduction were localized. The β and γ values were computed by the ratio of TVCD and surface concentration changes to 15% change of anthropogenic NO_x emissions, respectively.

Figure 2 shows the distributions of our β and γ ratios as a function of anthropogenic NO_x emissions for July 2011 over the CONUS. Results essentially the same as Figure 2 were obtained when a perturbation of 10% was used for anthropogenic NO_x emissions. Figure S6 shows the distributions of NO_2 TVCD fraction in the boundary layer at 13:00 – 14:00 LT and 10:00 – 11:00 LT, and the fraction of soil NO_x emissions in all surface sources (soil + anthropogenic) on weekdays for July 2011, respectively. In Figure S7, we analyzed the contributions of background sources and non-emission factors (transport, chemistry, and wet and dry depositions) to the nonlinear relationships (β and γ) among anthropogenic NO_x emissions, NO_2 surface concentrations, and NO_2 TVCDs. While the model simulation is for one summer month, several key points on the surface and column concentration sensitivities to anthropogenic NO_x emissions have implications for comparing the trends of AQS and satellite TVCD data. (1) Both β and γ values are negatively correlated with anthropogenic NO_x emissions due to chemical nonlinearity,

transport, and background NO_x contributions (Figures 2, S6, and S7) (Gu et al., 2016; Lamsal et al., 2011). It is consistent with the distribution of β as a function of NO_x emissions in China (Gu et al., 2013), although the β ratios for the US are generally larger than for China due primarily to different emission distributions of NO_x and VOCs and regional circulation patterns (Zhao et al., 2009b). (2) The uncertainties of β and γ values increase significantly as anthropogenic NO_x emissions decrease, which means regions with low anthropogenic NO_x emissions are more sensitive to environmental conditions, such as NO_x transport from nearby regions which may even produce negative β and γ values (Figures 2 and S7). (3) The value of γ is generally less than β, especially for low-anthropogenic-NO_x emission regions, which reflects the significant contribution of free tropospheric NO_2 to NO_2 TVCD but not to NO_2 surface concentrations (Figures 2, S6, and S7). (4) The variations of β and γ values in anthropogenic NO_x emission bins tend to be larger at 10:00 – 11:00 than at 13:00 – 14:00 LT, reflecting a stronger transport effect due to weaker chemical losses at 10:00 – 11:00 (Figure 2). (5) Both β and γ values are significantly less than 1 at 13:00 – 14:00 LT (β = 0.74 and γ = 0.84) when anthropogenic NO_x emissions are > 4×10^{12} molecules cm^{-2} s^{-1}, but they are close to 1 at 10:00 – 11:00 LT (β = 0.96 and γ = 1.02), which reflect stronger chemistry nonlinearity at 13:00 – 14:00 than in the morning (Figure 2). (6) Both background sources and non-emission factors contribute much more to β and γ values in low-anthropogenic-NO_x emission regions than in high-anthropogenic-NO_x emission regions (Figure S7). (7) Generally, non-emission factors contribute more to β and γ values than background sources in low-anthropogenic-NO_x emission regions (Figures S7c and S7d) except for the first bin where background sources contribute more to β and γ values than non-emission factors at 10:00 – 11:00, which is partly caused by some grid cells with extremely low anthropogenic NO_x emissions, increasing the mean contributions of background sources in the first bin.

The largely varying β and γ values for anthropogenic NO_x emissions < 10^{11} molecules cm^{-2} s^{-1} imply that the trends derived from satellite TVCD data do not directly represent anthropogenic NO_x emissions and that the variations of TVCD data may not be comparable to the corresponding surface NO_2 concentrations. We define a region "urban" if anthropogenic NO_x emissions from NEI2011 are > 10^{11} molecules cm^{-2} s^{-1}. All the other regions are defined as "rural". Figure 3 shows the distributions of anthropogenic NO_x emissions and urban and rural regions defined in this study. Such defined urban regions account for 69.8% of the total anthropogenic NO_x emissions over the CONUS, the trend of which is, therefore, representative of anthropogenic emission changes. A caveat is that some "urban" regions would become "rural" if anthropogenic NO_x emissions decreased after 2011 as the EPA anthropogenic NO_x emission trend suggested (Figure S21). In a sensitivity study, we define an urban region using a stricter criterion of anthropogenic NO_x emissions > 2 × 10^{11} molecules cm^{-2} s^{-1} and the analysis results are similar to those shown in the next section.

3.2 Trend comparisons between NO_2 AQS surface concentrations and coincident satellite NO_2 tropospheric VCD over urban and rural regions

By using anthropogenic NO_x emissions of 10^{11} molecules cm^{-2} s^{-1} as the threshold value, 157 AQS sites are urban, and the rest 22 sites are rural. Their properties are summarized in Table 2. Figure 4 shows the relative annual variations of AQS NO_2 surface measurements at 13:00 – 14:00 and coincident OMI-QA4ECV NO_2 TVCD data from 2005 – 2017 in each season for urban and rural regions. The contrast between the two regions is apparent in all seasons. For comparison purposes, we scale the time series of TVCD and AQS surface NO_2 to their corresponding 2005 values, and the resulting data are therefore unitless. Over urban regions, NO_2 surface concentrations are highly correlated with NO_2 TVCDs (TVCD = 1.03 × AQS + 0.11, R^2 = 0.98), reflecting the comparable and stable β and γ values (Figure 2). However, over rural regions, the scaled TVCD data significantly deviate from AQS NO_2 data (TVCD = 1.15 × AQS + 0.09, R^2 =

290 0.87). It is noteworthy that the discrepancies between urban and rural data are smaller in winter
291 than in spring, summer, and autumn due to a more dominant role of transport than chemistry and
292 lower natural NO_x emissions in winter.

293 We also examine the correlations of AQS NO_2 surface concentrations with coincident OMI-
294 NASA, OMI-BEHR, SCIAMACHY, GOME-2A, and GOME-2B TVCD measurements. The
295 results of OMI-NASA and OMI-BEHR are similar to those of OMI-QA4ECV (Figure 4).
296 SCIAMACHY and GOME-2B TVCD observations at 9:00-11:00 LT also show large contrast
297 between urban (SCIAMACHY: TVCD = 0.92 × AQS - 0.005, R^2 = 0.94; GOME-2B: TVCD =
298 0.54 × AQS + 0.56, R^2 = 0.96) and rural regions (SCIAMACHY: TVCD = 0.77 × AQS +0.83, R^2
299 = 0.63; GOME-2B: TVCD = 0.46 × AQS + 0.73, R^2 = 0.59). The correlation of coincident
300 GOME-2A NO_2 TVCD data with AQS surface concentrations is poor for rural (TVCD = 0.65 ×
301 AQS + 0.56, R^2 = 0.44) and urban (TVCD = 0.31 × AQS + 0.56, R^2 = 0.21) regions (Figure S8~~5~~),
302 which likely reflects the degradation of the GOME-2A instrument causing significant increase of
303 NO_2 SCD uncertainties (Boersma et al., 2018). Therefore, we excluded GOME-2A in the analysis
304 hereafter.

305 We further investigate ~~the sensitivities of~~ OMI-QA4ECV NO_2 TVCD relative annual
306 variations from 2005 - 2017 over the regions with~~to~~ different anthropogenic NO_x emissions ~~over~~
307 ~~the CONUS~~ in Figure 5. We find clear flattening of NO_2 TVCD variations as anthropogenic NO_x
308 emissions decrease, which is consistent with the above analysis. Similar to Figure 4, the spread of
309 TVCD variation is much less in winter than the other seasons. The differences between Figures 5
310 and 4 are due to a much larger dataset used in the former than the latter. Only coincident AQS
311 and OMI-QA4ECV data are used in Figure 4, but all OMI-KMNI data are used in Figure 5.

3.3 Trend analysis of AQS NO_2 surface concentrations, satellite TVCDs, and updated EPA NOx emissions

We first updated the CEMS measurement data used in the EPA NO_x emission trend datasets with the newest datasets obtained from https://ampd.epa.gov/ampd/. As shown in Figure S21, the updated CEMS data lead to a reduction of anthropogenic NO_x emissions during the Great Recession (2008 – 2009) and a recovery period in 2010 – 2011. The sharp drop during the Great Recession and the flattening trend right after the Great Recession are captured by OMI NO_2 and SCIAMACHY TVCD products (Figures 4, 6, and S96) and AQS NO_2 surface measurements (Figures 4, 6, and S54) and are also noted by Russell et al. (2012) and Tong et al. (2015) (Table 1).

In Figure 6, we show the comparisons among the relative variations of the updated EPA anthropogenic NO_x emissions, AQS NO_2 surface measurements at 10:00-11:00 and 13:00-14:00, and coincident satellite NO_2 TVCDs for urban regions in 4 seasons from 2003 to 2017. Also shown are the comparisons among the updated EPA anthropogenic NO_x emissions and satellite NO_2 TVCDs. There are many more data points for the latter comparison because the data selection is no longer limited to those coincident with the AQS surface data, and therefore, the uncertainty spread is much lower. The comparisons, in general, show consistent results that the updated EPA anthropogenic NO_x emissions, AQS surface measurements, and satellite TVCD data are in agreement. The agreement of decreasing trends among the datasets is just as good for the post-2011 period as the pre-2011 period. This result differs from Miyazaki et al. (2017) and Jiang et al. (2018), who suggested no significant decreasing trend for OMI TVCD data and inversed NO_x emissions after 2010. The disagreement can be explained by the results of Figure 5. Including the low anthropogenic NO_x emission regions leads to underestimates of NO_x decreases. Since the area of low anthropogenic NO_x emission regions is larger than high anthropogenic NO_x emission regions (Table 2), the arithmetic averaging will lead to a large weighting of rural

observations, which do not reflect anthropogenic NO_x emission changes. Miyazaki et al. (2017) and Jiang et al. (2018) included all regions in their analyses, but we exclude rural regions. Figure S~~9~~6 shows the seasonal variations if the TVCDs over rural regions are included; the result shows a much lower decreasing rate of TVCDs over the CONUS. The much slower satellite TVCD trends for regions with low NO_x emissions was previously discussed by Zhang et al. (2018). In addition, Miyazaki et al. (2017) and Jiang et al. (2018) conducted NO_x emission inversions by using the Model for Interdisciplinary Research on Climate (MIROC)-Chem with a coarse resolution of 2.8° × 2.8°, which was insufficient to separate urban and rural regions and might distort predicted NO_2 TVCDs and inversed NO_x emissions due to nonlinear effects (Valin et al., 2011; Yu et al., 2016), which is another possible reason for their find of flattening NO_x emission trends after 2010.

We summarize the decreasing rates of NO_2 after the Great Recession in Table 3. To minimize the effect of the sharp decrease and the subsequent recovery, we chose to analyze the post-2011 period. Table 3 summarizes the results for each season, while Table 1 gives the averaged annual decreasing trends. Generally, Tables 1 and 3 confirm the continuous decreases of AQS surface observations, satellite NO_2 TVCD, and updated EPA anthropogenic NO_x emissions after 2011 as in Figure 6, but the decreasing rates are lower than the pre-2011 period. Over the AQS urban sites, the slowdown magnitudes are 9% for AQS surface observations and 20% - 40% for satellite NO_2 TVCD measurements, which may reflect in part smaller γ than β values (Table 2). Our estimated slowdown magnitudes are significantly lower than Lamsal et al. (2015) and Jiang et al. (2018) ~~but comparable to the results by Tong et al. (2015)~~ (Table 1)~~. The agreement with Tong et al. (2015) is because we select urban AQS sites based on anthropogenic NO_x emissions and they chose eight large cities, while Lamsal et al. (2015) and Jiang et al. (2018) used all AQS sites.~~, which might be caused by their different data processing methods, such as including AQS sites with incomplete measurement records (Silvern et al., 2019).

Over the CONUS urban regions, updated EPA anthropogenic NO_x emissions show a slowdown of 22% compared to 29% - 46% for three OMI NO_2 TVCD products. The difference is partially due to the β ratio of 2.5~~3~~ ± 1.0~~0.9~~ at 13:00 – 14:00 over the CONUS urban regions (Table 2). Satellite NO_2 TVCD measurement uncertainties also contribute to the difference. From 2013 – 2017, GOME-2B NO_2 TVCDs decrease more than OMI products, especially in spring, autumn and winter (Tables 1 and 3). Finally, trend analyses in different regions (Figure 7 and Table S4) indicate that generally, the Midwest has the least slowdown of the decreasing rate for urban OMI NO_2 TVCD (-14% on average) after 2011 compared to the Northeast (-30%), South (-34%), and West (-28%).

The results presented in this study are qualitatively in agreement with the work by Silvern et al. (2019). The two studies were independent. Therefore, the foci of the studies are different despite reaching similar conclusions. While we focused on understanding the detailed data analysis of Jiang et al. (2018) and limited the use of model simulation results so that our results can be compared to the previous study directly, Silvern et al. (2019) relied more on multi-year model simulations. As a result, Silvern et al. (2019) can clearly identify the contributions of the NO_2 columns by natural emissions and make use of additional observations such as nitrate deposition fluxes. They also identified model biases in simulating the trends of NO_2 TVCDs by missing natural emissions in the free troposphere. Our study, on the other hand, explored the data analysis procedure through which the trend of anthropogenic emissions can be derived from satellite observations and its limitations.

4. Conclusions

Using model simulations for July 2017, we demonstrate the nonlinear relationship of NO_2 surface concentration and TVCD with anthropogenic NO_x emissions. Over low anthropogenic NO_x emission regions, the ratios of anthropogenic NO_x emission changes to the changes of

surface concentrations (γ) and TVCDs (β) have very large variations and $\beta > \gamma \gg 1$. Therefore, for the same emission changes, surface concentration and TVCD changes are much smaller and variable than urban regions, making it difficult to use the observations to directly infer anthropogenic NO_x emission trends. We find that defining urban regions where anthropogenic NO_x emissions are > 10^{11} molecules cm^{-2} s^{-1} and using surface and TVCD observations over these regions can infer the trends that can be compared with the EPA emission trend estimates.

We evaluate the anthropogenic NO_x emission variations from 2003 – 2017 over the CONUS by using satellite NO_2 TVCD products from GOME-2B, SCIAMACHY, OMI-QA4ECV, OMI-NASA, and OMI-BEHR, over the urban regions of CONUS. We find broad agreements among the decreases of AQS NO_2 surface observations, satellite NO_2 TVCD products, and the EPA anthropogenic NO_x emissions with the CEMS dataset updated. After 2011, they all show a slowdown of the decreasing rates. Over the AQS urban sites, NO_2 surface concentrations have a slowdown of 9% and OMI products show a slowdown of 20% - 40%. Over the CONUS urban regions, OMI TVCD products indicate a slowdown of 29% - 46%, and the updated EPA anthropogenic NO_x emissions have a slowdown of 22%. The different slowdown magnitudes between OMI TVCD products and the other two datasets may be caused by the nonlinear response of TVCD to anthropogenic emissions and the uncertainties of satellite measurements (e.g., GOME-2B TVCD data show a larger decreasing trend than OMI products from 2013 – 2017).

We did not find observation evidence supporting the notion that anthropogenic NO_x emissions have not been decreasing after the Great Recession. In future studies, we recommend that the nonlinear relationships of NO_x emissions with NO_2 TVCD and surface concentration be

carefully evaluated when applying satellite and surface measurements to infer the changes of anthropogenic NO_x emissions.

Data availability

The EPA AQS hourly surface NO_2 measurements are downloaded from https://aqs.epa.gov/aqsweb/airdata/download_files.html#Raw. QA4ECV 1.1 NO_2 VCD products (OMI-QA4ECV, GOME-2A, and SCIAMACHY) are from http://temis.nl/qa4ecv/no2col/data/. GOME-2B NO_2 VCD products are from http://www.temis.nl/airpollution/no2col/no2colgome2b.php. OMI-BEHR and OMI-NASA archives are from http://behr.cchem.berkeley.edu/DownloadBEHRData.aspx. REAM simulation results for this study are available upon request.

Author contribution

JL and YW designed the study. JL conducted model simulations and data analyses with discussions with YW. JL and YW wrote the manuscript.

Competing interests

The authors declare that they have no conflict of interest.

Acknowledgments

This work was supported by the NASA ACMAP Program. We thank Ruixiong Zhang for discussions with J. Li. Thank Benjamin Wells, Alison Eyth, Lee Tooly from EPA, the EPA MOVES team, Betty Carter from COORDINATING RESEARCH COUNCIL, INC., Brain McDonald from NOAA, and Zhe Jiang from University of Science and Technology of China for helping us an understanding of the NEI MOVES mobile source emissions.

References

Alkuwari, F. A., Guillas, S., and Wang, Y.: Statistical downscaling of an air quality model using Fitted Empirical Orthogonal Functions, Atmos. Environ., 81, 1-10, 10.1016/j.atmosenv.2013.08.031, 2013.

Beaver, M., Long, R., and Kronmiller, K.: Characterization and Development of Measurement Methods for Ambient Nitrogen Dioxide (NO_2), National Air Quality Conference - Ambient Air Monitoring 2012, Denver, CO, US, 2012.

Beaver, M., Kronmiller, K., Duvall, R., Kaushik, S., Morphy, T., King, P., and Long, R.: Direct and Indirect Methods for the Measurement of Ambient Nitrogen Dioxide, AWMA Measurement Technologies meeting, Sacramento, CA, US, 2013.

Beirle, S., Platt, U., Wenig, M., and Wagner, T.: Weekly cycle of NO_2 by GOME measurements: A signature of anthropogenic sources, Atmos. Chem. Phys., 3, 2225-2232, 10.5194/acp-3-2225-2003, 2003.

Bishop, G. A., and Stedman, D. H.: Reactive nitrogen species emission trends in three light-/medium-duty United States fleets, Environ. Sci. Technol., 49, 11234-11240, 10.1021/acs.est.5b02392, 2015.

Boersma, K. F., Eskes, H. J., Richter, A., De Smedt, I., Lorente, A., Beirle, S., van Geffen, J. H., Zara, M., Peters, E., and Roozendael, M. V.: Improving algorithms and uncertainty estimates for satellite NO_2 retrievals: results from the quality assurance for the essential climate variables (QA4ECV) project, Atmos. Meas. Tech., 11, 6651-6678, 10.5194/amt-11-6651-2018, 2018.

Cheng, Y., Wang, Y., Zhang, Y., Chen, G., Crawford, J. H., Kleb, M. M., Diskin, G. S., and Weinheimer, A. J.: Large biogenic contribution to boundary layer O_3-CO regression slope in summer, Geophys. Res. Lett., 44, 7061-7068, 10.1002/2017GL074405, 2017.

Cheng, Y., Wang, Y., Zhang, Y., Crawford, J. H., Diskin, G. S., Weinheimer, A. J., and Fried, A.: Estimator of surface ozone using formaldehyde and carbon monoxide concentrations over the eastern United States in summer, J. Geophys. Res.-Atmos., 123, 7642-7655, 10.1029/2018JD028452, 2018.

Choi, Y., Wang, Y., Zeng, T., Martin, R. V., Kurosu, T. P., and Chance, K.: Evidence of lightning NO_x and convective transport of pollutants in satellite observations over North America, Geophys. Res. Lett., 32, 10.1029/2004GL021436, 2005.

Choi, Y., Wang, Y., Yang, Q., Cunnold, D., Zeng, T., Shim, C., Luo, M., Eldering, A., Bucsela, E., and Gleason, J.: Spring to summer northward migration of high O_3 over the western North Atlantic, Geophys. Res. Lett., 35, 10.1029/2007GL032276, 2008a.

Choi, Y., Wang, Y., Zeng, T., Cunnold, D., Yang, E. S., Martin, R., Chance, K., Thouret, V., and Edgerton, E.: Springtime transitions of NO_2, CO, and O_3 over North America: Model evaluation and analysis, J. Geophys. Res.-Atmos., 113, 10.1029/2007JD009632, 2008b.

Choi, Y., Kim, H., Tong, D., and Lee, P.: Summertime weekly cycles of observed and modeled NO_x and O_3 concentrations as a function of satellite-derived ozone production sensitivity and land use types over the Continental United States, Atmos. Chem. Phys., 12, 6291-6307, 10.5194/acp-12-6291-2012, 2012.

Crouse, D. L., Peters, P. A., Hystad, P., Brook, J. R., van Donkelaar, A., Martin, R. V., Villeneuve, P. J., Jerrett, M., Goldberg, M. S., and Pope III, C. A.: Ambient $PM_{2.5}$, O_3, and NO_2 exposures and associations with mortality over 16 years of follow-up in the Canadian Census Health and Environment Cohort (CanCHEC), Environ. Health Perspect., 123, 1180, 10.1289/ehp.1409276, 2015.

De Gouw, J. A., Parrish, D. D., Frost, G. J., and Trainer, M.: Reduced emissions of CO2, NO_x, and SO_2 from US power plants owing to switch from coal to natural gas with combined cycle technology, Earth's Future, 2, 75-82, 10.1002/2013EF000196, 2014.

Drosoglou, T., Bais, A. F., Zyrichidou, I., Kouremeti, N., Poupkou, A., Liora, N., Giannaros, C., Koukouli, M. E., Balis, D., and Melas, D.: Comparisons of ground-based tropospheric NO_2 MAX-DOAS measurements to satellite observations with the aid of an air quality model over the Thessaloniki area, Greece, Atmos. Chem. Phys., 17, 5829-5849, 10.5194/acp-17-5829-2017, 2017.

Drosoglou, T., Koukouli, M. E., Kouremeti, N., Bais, A. F., Zyrichidou, I., Balis, D., Xu, J., and Li, A.: MAX-DOAS NO_2 observations over Guangzhou, China; ground-based and satellite comparisons, Atmos. Meas. Tech., 11, 2239-2255, 10.5194/amt-11-2239-2018, 2018.

EPA: PROFILE OF VERSION 1 OF THE 2014 NATIONAL EMISSIONS INVENTORY, U.S. Environmental Protection Agency, 2017.

Air Pollutant Emissions Trends Data: https://www.epa.gov/air-emissions-inventories/air-pollutant-emissions-trends-data, 2018.

Fisher, J. A., Jacob, D. J., Travis, K. R., Kim, P. S., Marais, E. A., Chan Miller, C., Yu, K., Zhu, L., Yantosca, R. M., and Sulprizio, M. P.: Organic nitrate chemistry and its implications for nitrogen budgets in an isoprene-and monoterpene-rich atmosphere: constraints from aircraft ($SEAC^4RS$) and ground-based (SOAS) observations in the Southeast US, Atmos. Chem. Phys., 16, 5969-5991, 10.5194/acp-16-5969-2016, 2016.

Georgoulias, A. K., van der A, R. J., Stammes, P., Boersma, K. F., and Eskes, H. J.: Trends and trend reversal detection in 2 decades of tropospheric NO_2 satellite observations, Atmos. Chem. Phys., 19, 6269-6294, 10.5194/acp-19-6269-2019, 2019.

Greenberg, N., Carel, R. S., Derazne, E., Bibi, H., Shpriz, M., Tzur, D., and Portnov, B. A.: Different effects of long-term exposures to SO_2 and NO_2 air pollutants on asthma severity in young adults, J. Toxicol. Environ. Health, A, 79, 342-351, 10.1080/15287394.2016.1153548, 2016.

Greenberg, N., Carel, R. S., Derazne, E., Tiktinsky, A., Tzur, D., and Portnov, B. A.: Modeling long-term effects attributed to nitrogen dioxide (NO_2) and sulfur dioxide (SO_2) exposure on asthma morbidity in a nationwide cohort in Israel, J. Toxicol. Environ. Health, A, 80, 326-337, 10.1080/15287394.2017.1313800, 2017.

Gu, D., Wang, Y., Smeltzer, C., and Liu, Z.: Reduction in NO_x emission trends over China: Regional and seasonal variations, Environ. Sci. Technol., 47, 12912-12919, 10.1021/es401727e, 2013.

Gu, D., Wang, Y., Smeltzer, C., and Boersma, K. F.: Anthropogenic emissions of NO_x over China: Reconciling the difference of inverse modeling results using GOME-2 and OMI measurements, J. Geophys. Res.-Atmos., 119, 7732-7740, 10.1002/2014JD021644, 2014.

Gu, D., Wang, Y., Yin, R., Zhang, Y., and Smeltzer, C.: Inverse modelling of NO_x emissions over eastern China: uncertainties due to chemical non-linearity, Atmos. Meas. Tech., 9, 5193-5201, 10.5194/amt-9-5193-2016, 2016.

Guenther, A. B., Jiang, X., Heald, C. L., Sakulyanontvittaya, T., Duhl, T., Emmons, L. K., and Wang, X.: The Model of Emissions of Gases and Aerosols from Nature version 2.1 (MEGAN2.1): an extended and updated framework for modeling biogenic emissions, Geosci. Model Dev., 5, 1471-1492, 10.5194/gmd-5-1471-2012, 2012.

Hassler, B., McDonald, B. C., Frost, G. J., Borbon, A., Carslaw, D. C., Civerolo, K., Granier, C., Monks, P. S., Monks, S., and Parrish, D. D.: Analysis of long-term observations of NO_x and CO in megacities and application to constraining emissions inventories, Geophys. Res. Lett., 43, 9920-9930, 10.1002/2016GL069894, 2016.

Heinrich, J., Thiering, E., Rzehak, P., Krämer, U., Hochadel, M., Rauchfuss, K. M., Gehring, U., and Wichmann, H.-E.: Long-term exposure to NO_2 and PM_{10} and all-cause and cause-specific mortality in a prospective cohort of women, Occup. Environ. Med., 70, 179-186, 10.1136/oemed-2012-100876, 2013.

Jiang, Z., McDonald, B. C., Worden, H., Worden, J. R., Miyazaki, K., Qu, Z., Henze, D. K., Jones, D. B. A., Arellano, A. F., and Fischer, E. V.: Unexpected slowdown of US pollutant emission reduction in the past decade, Proc. Natl. Acad. Sci. U.S.A., 201801191, 10.1073/pnas.1801191115, 2018.

Kampa, M., and Castanas, E.: Human health effects of air pollution, Environ. Pollut., 151, 362-367, 10.1016/j.envpol.2007.06.012, 2008.

Kebabian, P. L., Herndon, S. C., and Freedman, A.: Detection of nitrogen dioxide by cavity attenuated phase shift spectroscopy, Anal. Chem., 77, 724-728, 10.1021/ac048715y, 2005.

Koo, J.-H., Wang, Y., Kurosu, T. P., Chance, K., Rozanov, A., Richter, A., Oltmans, S. J., Thompson, A. M., Hair, J. W., and Fenn, M. A.: Characteristics of tropospheric ozone depletion events in the Arctic spring: analysis of the ARCTAS, ARCPAC, and ARCIONS measurements and satellite BrO observations, Atmos. Chem. Phys., 12, 9909-9922, 10.5194/acp-12-9909-2012, 2012.

Krotkov, N. A., Lamsal, L. N., Celarier, E. A., Swartz, W. H., Marchenko, S. V., Bucsela, E. J., Chan, K. L., Wenig, M., and Zara, M.: The version 3 OMI NO_2 standard product, Atmos. Meas. Tech., 10, 3133-3149, 10.5194/amt-10-3133-2017, 2017.

Lamsal, L. N., Martin, R. V., Padmanabhan, A., Van Donkelaar, A., Zhang, Q., Sioris, C. E., Chance, K., Kurosu, T. P., and Newchurch, M. J.: Application of satellite observations for timely

updates to global anthropogenic NO_x emission inventories, Geophys. Res. Lett., 38, 10.1029/2010GL046476, 2011.

Lamsal, L. N., Duncan, B. N., Yoshida, Y., Krotkov, N. A., Pickering, K. E., Streets, D. G., and Lu, Z.: US NO_2 trends (2005–2013): EPA Air Quality System (AQS) data versus improved observations from the Ozone Monitoring Instrument (OMI), Atmos. Environ., 110, 130-143, 10.1016/j.atmosenv.2015.03.055, 2015.

Laughner, J. L., Zhu, Q., and Cohen, R. C.: The Berkeley High Resolution Tropospheric NO_2 product, Earth System Science Data, 10, 2069-2095, 10.5194/essd-10-2069-2018, 2018.

Li, J., Mao, J., Fiore, A. M., Cohen, R. C., Crounse, J. D., Teng, A. P., Wennberg, P. O., Lee, B. H., Lopez-Hilfiker, F. D., and Thornton, J. A.: Decadal changes in summertime reactive oxidized nitrogen and surface ozone over the Southeast United States, Atmos. Chem. Phys., 18, 2341-2361, 10.5194/acp-18-2341-2018, 2018.

Li, J., Wang, Y., and Qu, H.: Dependence of summertime surface ozone on NO_x and VOC emissions over the United States: Peak time and value, Geophys. Res. Lett., 46, 3540-3550, 10.1029/2018GL081823, 2019.

Liu, Z., Wang, Y., Vrekoussis, M., Richter, A., Wittrock, F., Burrows, J. P., Shao, M., Chang, C. C., Liu, S. C., and Wang, H.: Exploring the missing source of glyoxal (CHOCHO) over China, Geophys. Res. Lett., 39, 10.1029/2012GL051645, 2012.

Liu, Z., Wang, Y., Costabile, F., Amoroso, A., Zhao, C., Huey, L. G., Stickel, R., Liao, J., and Zhu, T.: Evidence of aerosols as a media for rapid daytime HONO production over China, Environ. Sci. Technol., 48, 14386-14391, 10.1021/es504163z, 2014.

Luo, C., Wang, Y., and Koshak, W. J.: Development of a self-consistent lightning NO_x simulation in large-scale 3-D models, J. Geophys. Res.-Atmos., 122, 3141-3154, 10.1002/2016JD026225, 2017.

McDonald, B., McKeen, S., Cui, Y. Y., Ahmadov, R., Kim, S.-W., Frost, G. J., Pollack, I., Peischl, J., Ryerson, T. B., and Holloway, J.: Modeling Ozone in the Eastern US using a Fuel-Based Mobile Source Emissions Inventory, Environ. Sci. Technol., 10.1021/acs.est.8b00778, 2018.

Miyazaki, K., Eskes, H., Sudo, K., Boersma, K. F., Bowman, K., and Kanaya, Y.: Decadal changes in global surface NO_x emissions from multi-constituent satellite data assimilation, Atmos. Chem. Phys, 17, 807-837, 10.5194/acp-17-807-2017, 2017.

Myhre, G., Shindell, D., Bréon, F.-M., Collins, W., Fuglestvedt, J., Huang, J., Koch, D., Lamarque, J.-F., Lee, D., Mendoza, B., Nakajima, T., Robock, A., Stephens, G., Takemura, T., and Zhang, H.: Anthropogenic and natural radiative forcing, in: Climate change 2013: The Physical Science Basis. Contribution of Working Group I to the Fifth Assessment Report of the Intergovernmental Panel on Climate Change, Cambridge University Press, Cambridge, United Kingdom and New York, NY, USA, 659-740, 2013.

Pandey, J. S., Kumar, R., and Devotta, S.: Health risks of NO_2, SPM and SO_2 in Delhi (India), Atmos. Environ., 39, 6868-6874, 10.1016/j.atmosenv.2005.08.004, 2005.

584 Price, C., and Rind, D.: A simple lightning parameterization for calculating global lightning
585 distributions, J. Geophys. Res.-Atmos., 97, 9919-9933, 10.1029/92JD00719, 1992.

586 Russell, A. R., Valin, L. C., and Cohen, R. C.: Trends in OMI NO_2 observations over the United
587 States: effects of emission control technology and the economic recession, Atmos. Chem. Phys.,
588 12, 12197-12209, 10.5194/acp-12-12197-2012, 2012.

589 Seinfeld, J. H., and Pandis, S. N.: Atmospheric chemistry and physics: from air pollution to
590 climate change, John Wiley & Sons, Inc, Hoboken, New Jersey, 2016.

591 Silvern, R. F., Jacob, D. J., Mickley, L. J., Sulprizio, M. P., Travis, K. R., Marais, E. A., Cohen,
592 R. C., Laughner, J. L., Choi, S., Joiner, J., and Lamsal, L. N.: Using satellite observations of
593 tropospheric NO_2 columns to infer long-term trends in US NO_x emissions: the importance of
594 accounting for the free tropospheric NO_2 background, Atmos. Chem. Phys., 19, 8863-8878,
595 10.5194/acp-19-8863-2019, 2019.

596 Singh, A., and Agrawal, M.: Acid rain and its ecological consequences, J. Environ. Biol., 29, 15,
597 2007.

598 Tong, D., Lamsal, L., Pan, L., Ding, C., Kim, H., Lee, P., Chai, T., Pickering, K. E., and Stajner,
599 I.: Long-term NO_x trends over large cities in the United States during the great recession:
600 Comparison of satellite retrievals, ground observations, and emission inventories, Atmos.
601 Environ., 107, 70-84, 10.1016/j.atmosenv.2015.01.035, 2015.

602 Valin, L. C., Russell, A. R., Hudman, R. C., and Cohen, R. C.: Effects of model resolution on the
603 interpretation of satellite NO_2 observations, Atmos. Chem. Phys., 11, 11647-11655, 10.5194/acp-
604 11-11647-2011, 2011.

605 Wang, Y., Choi, Y., Zeng, T., Davis, D., Buhr, M., Huey, L. G., and Neff, W.: Assessing the
606 photochemical impact of snow NO_x emissions over Antarctica during ANTCI 2003, Atmos.
607 Environ., 41, 3944-3958, 10.1016/j.atmosenv.2007.01.056, 2007.

608 Wang, Y., Beirle, S., Lampel, J., Koukouli, M., De Smedt, I., Theys, N., Ang, L., Wu, D., Xie, P.,
609 and Liu, C.: Validation of OMI, GOME-2A and GOME-2B tropospheric NO_2, SO_2 and HCHO
610 products using MAX-DOAS observations from 2011 to 2014 in Wuxi, China: investigation of the
611 effects of priori profiles and aerosols on the satellite products, Atmos. Chem. Phys., 17, 5007,
612 10.5194/acp-17-5007-2017, 2017.

613 Weinmayr, G., Romeo, E., De Sario, M., Weiland, S. K., and Forastiere, F.: Short-term effects of
614 PM_{10} and NO_2 on respiratory health among children with asthma or asthma-like symptoms: a
615 systematic review and meta-analysis, Environ. Health Perspect., 118, 449-457,
616 10.1289/ehp.0900844, 2009.

617 Xing, J., Pleim, J., Mathur, R., Pouliot, G., Hogrefe, C., Gan, C. M., and Wei, C.: Historical
618 gaseous and primary aerosol emissions in the United States from 1990 to 2010, Atmos. Chem.
619 Phys., 13, 7531-7549, 10.5194/acp-13-7531-2013, 2013.

620 Yang, Q., Wang, Y., Zhao, C., Liu, Z., Gustafson Jr, W. I., and Shao, M.: NO_x emission reduction
621 and its effects on ozone during the 2008 Olympic Games, Environ. Sci. Technol., 45, 6404-6410,
622 10.1021/es200675v, 2011.

Yienger, J. J., and Levy, H.: Empirical model of global soil-biogenic NO_x emissions, J. Geophys. Res.-Atmos., 100, 11447-11464, 10.1029/95JD00370, 1995.

Yu, K., Jacob, D. J., Fisher, J. A., Kim, P. S., Marais, E. A., Miller, C. C., Travis, K. R., Zhu, L., Yantosca, R. M., and Sulprizio, M. P.: Sensitivity to grid resolution in the ability of a chemical transport model to simulate observed oxidant chemistry under high-isoprene conditions, Atmos. Chem. Phys., 16, 4369-4378, 10.5194/acp-16-4369-2016, 2016.

Zara, M., Boersma, K. F., De Smedt, I., Richter, A., Peters, E., Van Geffen, J. H. G. M., Beirle, S., Wagner, T., Van Roozendael, M., and Marchenko, S.: Improved slant column density retrieval of nitrogen dioxide and formaldehyde for OMI and GOME-2A from QA4ECV: intercomparison, uncertainty characterization, and trends, Meas. Tech. Discuss, 1-47, 10.5194/amt-11-4033-2018, 2018.

Zhang, R., Wang, Y., He, Q., Chen, L., Zhang, Y., Qu, H., Smeltzer, C., Li, J., Alvarado, L., and Vrekoussis, M.: Enhanced trans-Himalaya pollution transport to the Tibetan Plateau by cut-off low systems, Atmos. Chem. Phys., 17, 3083-3095, 10.5194/acp-17-3083-2017, 2017.

Zhang, R., Wang, Y., Smeltzer, C., Qu, H., Koshak, W., and Boersma, K. F.: Comparing OMI-based and EPA AQS in situ NO_2 trends: towards understanding surface NO_x emission changes, Atmos. Meas. Tech., 11, 3955-3967, 10.5194/amt-11-3955-2018, 2018.

Zhang, Y., and Wang, Y.: Climate-driven ground-level ozone extreme in the fall over the Southeast United States, Proc. Natl. Acad. Sci. U.S.A., 113, 10025-10030, 10.1073/pnas.1602563113, 2016.

Zhao, C., and Wang, Y.: Assimilated inversion of NO_x emissions over east Asia using OMI NO_2 column measurements, Geophys. Res. Lett., 36, 10.1029/2008GL037123, 2009.

Zhao, C., Wang, Y., Choi, Y., and Zeng, T.: Summertime impact of convective transport and lightning NO_x production over North America: modeling dependence on meteorological simulations, Atmos. Chem. Phys., 9, 4315-4327, 10.5194/acp-9-4315-2009, 2009a.

Zhao, C., Wang, Y., and Zeng, T.: East China plains: A "basin" of ozone pollution, Environ. Sci. Technol., 43, 1911-1915, 10.1021/es8027764, 2009b.

Zhao, C., Wang, Y., Yang, Q., Fu, R., Cunnold, D., and Choi, Y.: Impact of East Asian summer monsoon on the air quality over China: View from space, J. Geophys. Res.-Atmos., 115, 10.1029/2009JD012745, 2010.

Table 1. Summary of trends of satellite NO_2 TVCD products, NO_2 surface measurements, and EPA anthropogenic NO_x emissions during from different studies

Studies	Datasets	Period 1[1]		Period 2		Period 3		Slowdown ratio[3]
		Time	Trend (yr^{-1})[2]	Time	Trend (yr^{-1})	Time	Trend (yr^{-1})	
This study for CONUS "urban" sites[4]	GOME-2B[5] (36 × 36 km^2)					2013 - 2017	**-8.2 ± 3.0%**	
	SCIAMACHY (36 × 36 km^2)	2003 – 2011	**-6.3 ± 1.1%**					
	OMI-NASA (36 × 36 km^2)	2005 – 2011	**-8.6 ± 1.2%**			2011 – 2016	**-6.1 ± 3.6%**	**-29%**[2]
	OMI-BEHR (36 × 36 km^2)	2005 – 2011	**-8.2 ± 1.3%**			2011 – 2016	**-4.4 ± 1.6%**	**-46%**
	OMI-QA4ECV (36 × 36 km^2)	2005 – 2011	**-7.7 ± 1.4%**			2011 - 2017	**-4.2 ± 0.5%**	**-46%**
	Updated EPA NO_x emissions[6]	2003 – 2011	**-6.5 ± 0.8%**			2011 - 2017	**-5.1 ± 0.3%**	**-22%**
This study for AQS "urban" sites	GOME-2B (36 × 36 km^2)					2013 - 2017	**-10.2 ± 2.9%**	
	SCIAMACHY (36 × 36 km^2)	2003 - 2011	**-7.6 ± 1.1%**					
	OMI-NASA (36 × 36 km^2)	2005 - 2011	**-9.0 ± 0.8%**			2011 – 2016	**-7.2 ± 3.8%**	**-20%**
	OMI-BEHR (36 × 36 km^2)	2005 - 2011	**-8.9 ± 0.3%**			2011 – 2016	**-6.2 ± 2.6%**	**-30%**
	OMI-QA4ECV (36 × 36 km^2)	2005 - 2011	**-9.0 ± 0.8%**			2011 - 2017	**-5.4 ± 0.9%**	**-40%**
	NO_2 surface VMR[7]	2003 - 2011	**-6.5 ± 1.2%**			2011 - 2017	**-5.9 ± 0.8%**	**-9%**
(Russell et al., 2012)[8]	BEHR v2.1 NO_2 TVCD (0.05°×0.05°)	2005 - 2007	-6 ± 5% **(-6.2%)**[9]	2007 - 2009	-8 ± 5% **(-8.4%)**	2009 - 2011	-3 ± 4% **(-3.0%)**	**-52%**
	Updated EPA NO_x emissions		**-6.0%**		**-10.0%**		**-2.4%**	**-60%**
(Tong et al., 2015)[10]	NASA v2.1 NO_2 TVCD (pixels < 50 × 24 km^2)	2005 - 2007	-7.3% **(-7.6%)**	2008 - 2009	-9.2% **(-11.4%)**	2010 - 2012	-2.8% **(-4.4%)**	**-42%**
	BEHR v2.1 NO_2 TVCD (pixels < 50 × 24 km^2)		-8.9% **(-9.3%)**		-9.1% **(-11.8%)**		-3.6% **(-6.0%)**	**-35%**
	NO_2 surface VMR		-6.0% **(-6.2%)**		-10.8% **(-13.2%)**		-3.4% **(-5.4%)**	**-13%**
	Updated EPA NO_x emissions		**-6.0%**		**-10.0%**		**-3.4%**	**-43%**
(Lamsal et al., 2015)[11]	NASA v2.1 NO_2 TVCD (0.1°×0.1°)	2005 - 2008	-4.8 ± 1.9% **(-5.1%)**			2010 - 2013	-1.2 ± 1.2% **(-1.2%)**	**-76%**
	NO_2 surface VMR		-3.7 ± 1.5% **(-3.8%)**				-2.1 ± 1.4% **(-2.1%)**	**-45%**
	Updated EPA NO_x emissions		**-6.4%**				**-4.0%**	**-38%**
(Jiang et al., 2018)[11]	NASA v3 NO_2 TVCD (0.5°×0.667°)	2005 - 2009	-10.2 ± 1.8% **(-9.8%)**			2011-2015	-3.2 ± 1.6% **(-3.2%)**	**-67%**
	QA4ECV v2 NO_2 TVCD (0.5°×0.667°)		-9.6 ± 1.7% **(-9.3%)**				-2.6 ± 1.8% **(-2.6%)**	**-72%**
	BEHR v2.1 NO_2 TVCD (0.5°×0.667°)		-8.5 ± 1.8% **(-8.2%)**				-2.1 ± 1.6% **(-2.1%)**	**-74%**
	NO_2 surface VMR		-6.6 ± 1.4% **(-6.4%)**				-2.6 ± 1.5% **(-2.6%)**	**-59%**
	Updated EPA NO_x emissions		**-7.8%**				**-5.0%**	**-36%**

[1] Since different studies used different time division methods, we list the period of each study in the table.
[2] Trends are based on an exponential model ($E(y) = E_0 \times r^{y-y_0}$: "$y$" denotes year and "$y_0$" denotes the initial year; "$E(y)$" denotes the value at year "y" and "E_0" denotes the value at the initial year; r-1 is the relative trend).
[3] Slowdown ratios = Trend in "period 3" / Trend in "period 1" – 1.
[4] Trends in our study are calculated based on the national seasonal trends shown in Table 3.
[5] The information on satellite products used in this study is summarized in Table S2.
[6] We updated EPA anthropogenic NO_x emissions with the newest Continuous Emission Monitoring Systems (CEMS) datasets. Figure S2~~1~~ shows the comparison between our updated and original EPA anthropogenic NO_x emissions (EPA, 2018).
[7] Denote the averaged trends of 13:00 and 10:00 LT based on the values in Table 3.

[8] The study used NO_2 TVCD from urban and power plant grid cells across the U.S.

[9] Since previous studies used linear models to calculate trends and the results are sensitive to their calculation methods and the selection of initial years, we recalculate the trends based on the above exponential model, which makes all the results consistent. Our results are those bold numbers inside the parentheses, while the numbers in normal fonts are from the original publications.

[10] The study uses NO_2 TVCD and surface concentrations from Los Angeles, Dallas, Houston, Atlanta, Philadelphia, Washington, D.C., New York, and Boston.

[11] The two studies used the EPA Air Quality System (AQS) NO_2 surface measurements and coincident satellite NO_2 TVCD data over the U.S.

Table 2. Properties of urban and rural regions in July 2011

type	Surface area fraction[1]	Anthropogenic NO_x emissions ($\times 10^{10}$ molecules cm^{-2} s^{-1})	β at 13:00 – 14:00 LT	γ at 13:00 – 14:00 LT	β at 10:00 – 11:00 LT	γ at 10:00 – 11:00 LT
Urban/CONUS[2]	17.3%	29.9	2.53 ± 1.00.9	1.54 ± 0.43	2.64 ± 1.98	1.65 ± 1.20
Rural/CONUS	82.7%	2.7	16.98.1 ± 16.48.7	8.53.1 ± 11.73.9	12.25.9 ± 14.08.0	6.42.8 ± 11.65.8
Urban/AQS	87.7%	71.0	1.65 ± 0.87	1.2 ± 0.4	1.7 ± 1.10	1.3 ± 0.65
Rural/AQS	12.3%	5.7	8.75.0 ± 9.92.0	5.22.5 ± 8.81.3	5.44.3 ± 15.13.2	3.82.7 ± 11.72.6

[1] "Fraction" denotes the percentages of "urban" or "rural" data points for the whole CONUS or all AQS sites.
[2] "Urban-CONUS" denote CONUS "urban" grid cells; "Urban-AQS" denote AQS "urban" site grid cells.

Table 3. Summary of national trends of updated EPA anthropogenic NO_x emissions, AQS NO_2 surface concentrations at 13:00 – 14:00 and 10:00 – 11:00 LT, and satellite NO_2 TVCD products for 4 seasons during different periods[1]

		Spring		Summer		Autumn		Winter	
		AQS site	CONUS	AQS site	CONUS	AQS site	CONUS	AQS site	CONUS
AQS NO_2 VMR at 13:00 -14:00	2003 – 2011	-7.3 ± 1.4%		-7.4 ± 0.9%		-6.7 ± 1.8%		-5.2 ± 0.8%	
	2011 – 2017	-5.3 ± 1.6%		-6.4 ± 1.2%		-7.3 ± 2.5%		-6.0 ± 2.8%	
AQS NO_2 VMR at 10:00 – 11:00	2003 – 2011	-7.1 ± 1.6%		-7.6 ± 1.5%		-6.2 ± 2.2%		-4.4 ± 1.6%	
	2011 – 2017	-4.4 ± 1.4%		-6.1 ± 1.8%		-6.3 ± 2.5%		-5.2 ± 2.4%	
SCIAMACHY	2003 – 2011	-8.8 ± 3.4%	-6.9 ± 1.1%	-8.2 ± 1.6%	-5.2 ± 1.2%	-6.8 ± 2.4%	-5.6 ± 2.1%	-6.4 ± 7.4%	-7.5 ± 5.5%
	2011 – 2017								
GOME2B	2003 – 2011								
	2013 – 2017	-10.2 ± 7.8%	-8.3 ± 16.9%	-6.4 ± 14.0%	-5.3 ± 4.0%	-10.5 ± 41.6%	-6.9 ± 13.2%	-13.6 ± 15.1%	-12.3 ± 78.9%
OMI-QA4ECV	2005 – 2011	-9.3 ± 5.6%	-8.3 ± 4.6%	-8.3 ± 2.4%	-5.9 ± 5.2%	-10.0 ± 4.2%	-7.4 ± 2.4%	-8.3 ± 2.1%	-9.3 ± 5.2%
	2011 – 2017	-5.3 ± 6.0%	-4.3 ± 6.5%	-4.2 ± 3.0%	-4.9 ± 9.2%	-6.0 ± 1.8%	-3.8 ± 1.8%	-6.1 ± 25.6%	-3.8 ± 3.5%
OMI-NASA	2005 – 2011	-9.4 ± 5.0%	-9.6 ± 5.3%	-9.4 ± 2.8%	-7.1 ± 2.9%	-9.4 ± 3.2%	-8.1 ± 2.8%	-7.8 ± 3.6%	-9.5 ± 16.6%
	2011 – 2016	-4.4 ± 18.9%	-3.8 ± 7.5%	-5.7 ± 6.7%	-4.5 ± 5.3%	-6.0 ± 3.1%	-4.6 ± 3.9%	-12.8 ± 7.8%	-11.4 ± 6.6%
OMI-BEHR	2005 – 2011	-9.1 ± 5.3%	-8.9 ± 5.8%	-8.7 ± 2.4%	-6.4 ± 3.2%	-9.2 ± 3.2%	-8.0 ± 3.1%	-8.5 ± 10.6%	-9.4 ± 23.0%
	2011 – 2016	-3.8 ± 4.4%	-3.0 ± 4.0%	-5.4 ± 7.0%	-3.9 ± 6.6%	-5.6 ± 13.2%	-4.1 ± 14.0%	-9.9 ± 5.2%	-6.7 ± 5.9%
EPA	2003 – 2011				-6.5 ± 0.8%				
	2011 – 2017				-5.1 ± 0.3%				

[1] We calculate trends by using the exponential model described in Table 1.

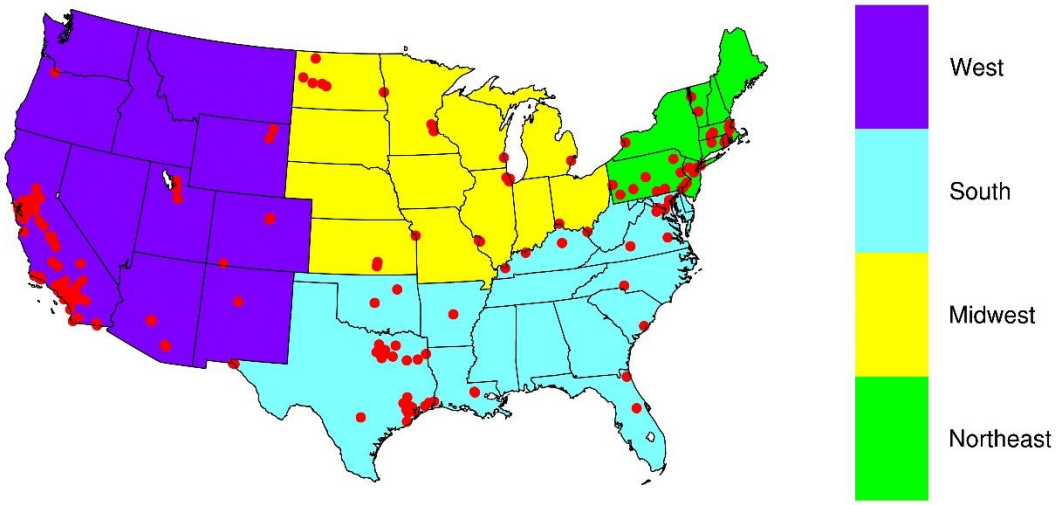

675
676 Figure 1. Region definitions and locations of NO_2 surface observation sites used in this study.

677

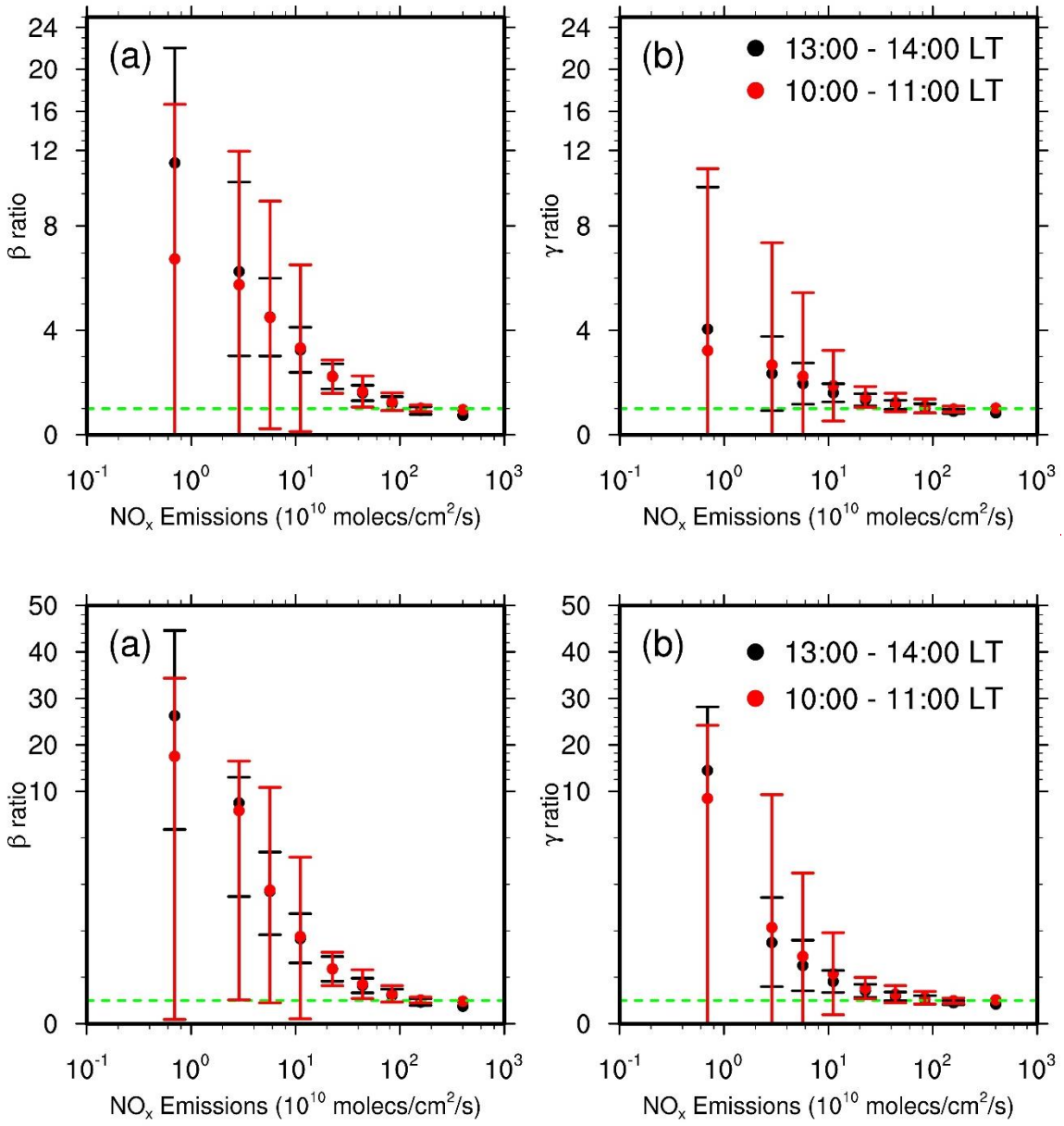

Figure 2. Distributions of β (panel a) and γ (panel b) ratios as a function of anthropogenic NO_x emissions on weekdays for July 2011 over the CONUS. "13:00 – 14:00 LT" is for OMI, and "10:00 – 11:00" LT is for SCIAMACHY and GOME-2A/2B. The data are binned into nine groups based on anthropogenic NO_x emissions: $E \in (0, 2^1)$, $[2^1, 2^2)$, $[2^2, 2^3)$, $[2^3, 2^4)$, $[2^4, 2^5)$, $[2^5, 2^6)$, $[2^6, 2^7)$, $[2^7, 2^8)$, $[2^8, 2^9) \times 10^{10}$ molecules cm^{-2} s^{-1}. Here, $(0, 2^1)$ denotes $0 <$ emissions $< 2^1$, and $[2^1, 2^2)$ denotes $2^1 \leq$ emissions $< 2^2$, similar to other intervals. The green dashed line denotes a value of 1. Error bars denote standard deviations.

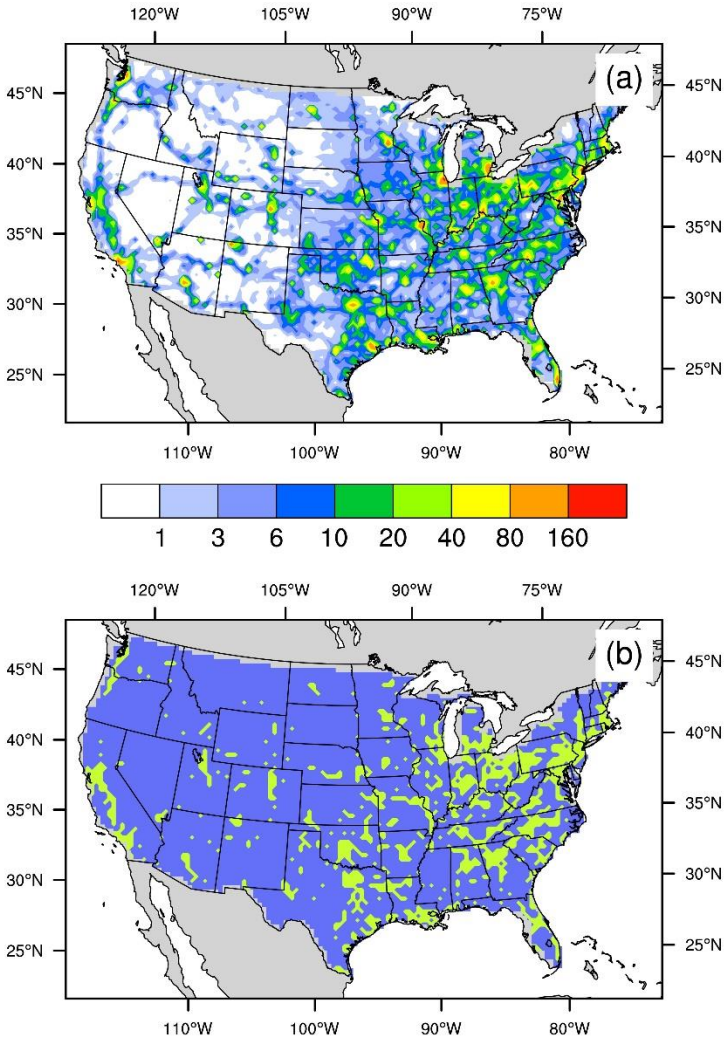

689
690 Figure 3. Spatial distributions of (a) anthropogenic NO_x emissions (unit: 10^{10} molecules cm^{-2} s^{-1})
691 and (b) "urban" regions satisfying our selection criteria. In (b), light green and blue denote the
692 resulting urban and rural regions, respectively.

693

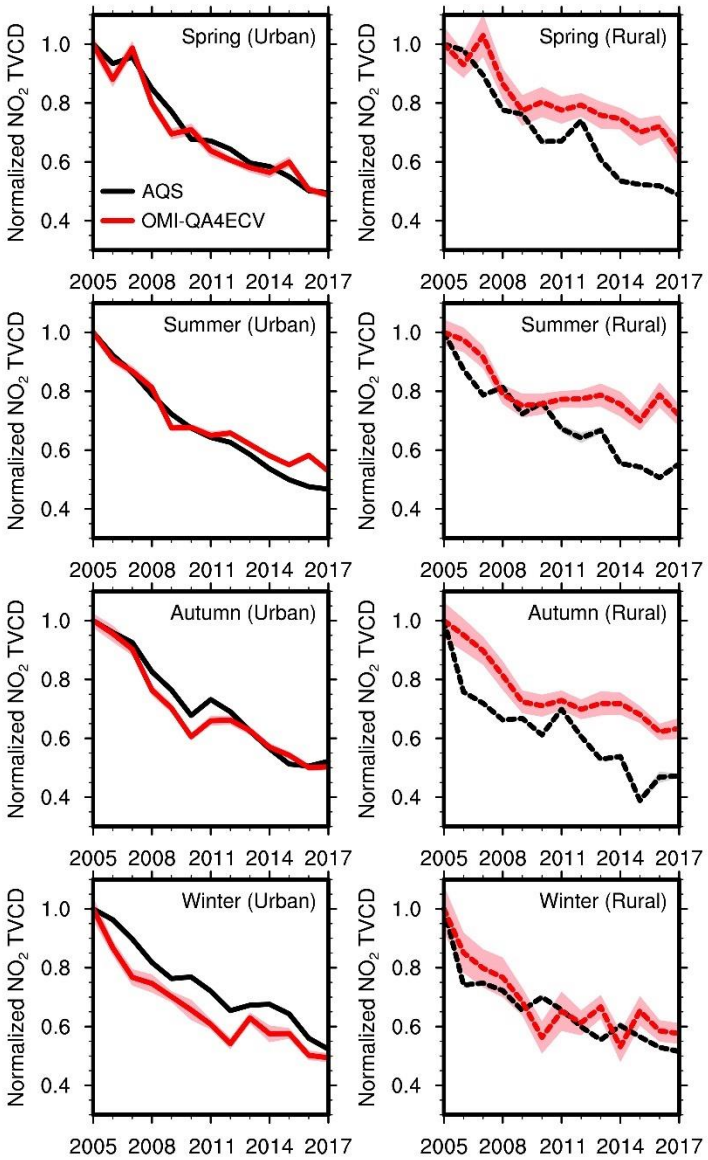

Figure 4. Relative annual variations of AQS NO_2 surface concentrations and coincident OMI-QA4ECV NO_2 TVCD in each season from 2005 – 2017 for urban (left panel) and rural (right panel) regions. The observation data are scaled by the corresponding 2005 values. Black and red lines denote AQS surface observations and OMI-QA4ECV NO_2 TVCDs, respectively. Shading in a lighter color is added to show the standard deviation of the results; when uncertainty is small due in part to a large number of data points, shading area may not show up.

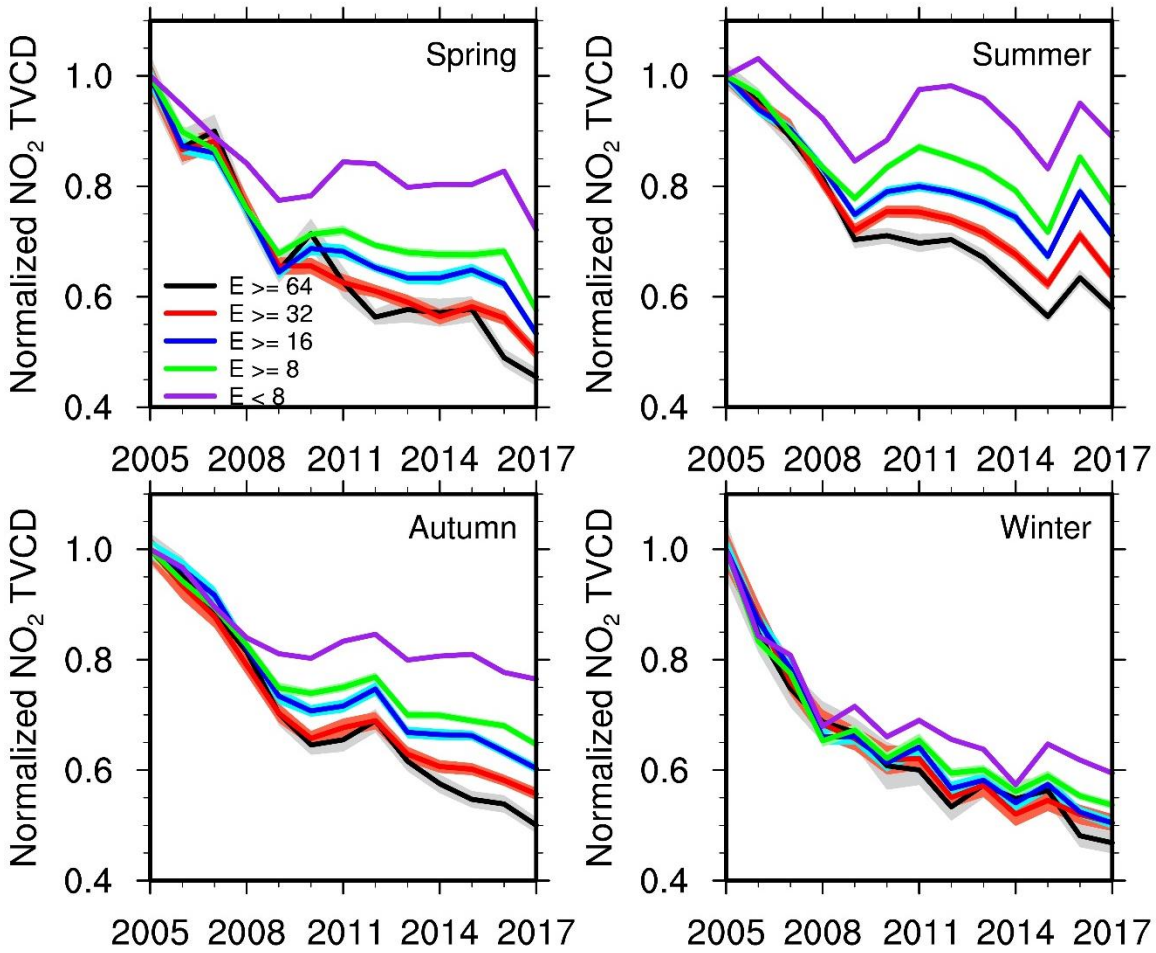

Figure 5. Relative annual variations of OMI-QA4ECV NO_2 TVCD for different anthropogenic NO_x-emission groups based on NEI2011 in each season from 2005 – 2017. "E >= 64" denotes grid cells with anthropogenic NO_x emissions over 64×10^{10} molecules cm^{-2} s^{-1}. "E >= 32" denotes grid cells with anthropogenic NO_x emissions equal to or larger than 32×10^{10} molecules cm^{-2} s^{-1} but less than 64×10^{10} molecules cm^{-2} s^{-1}. "E >= 16" and "E >= 8" have similar meanings as "E >= 32". "E < 8" denotes grid cells with anthropogenic NO_x emissions less than 8×10^{10} molecules cm^{-2} s^{-1}. Shading in a lighter color is added to show the standard deviation of the results; when uncertainty is small due in part to a large number of data points, shading area may not show up.

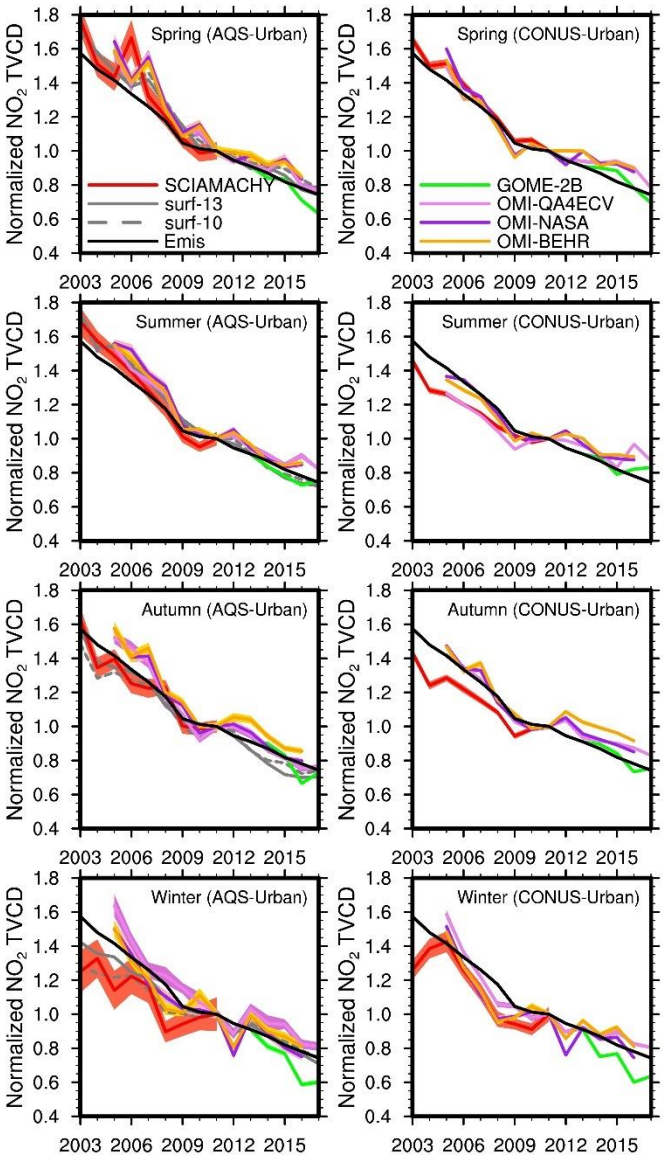

Figure 6. Relative variations of AQS NO_2 surface measurements at 13:00-14:00 and 10:00-11:00 LT, updated EPA anthropogenic NO_x emissions, and satellite NO_2 TVCD data over the AQS urban sites (left column) and the CONUS urban regions (right column) for 4 seasons. AQS NO_2 surface measurements are not included in the right column. All datasets are scaled by their corresponding values in 2011 except for GOME-2B. For GOME-2B, we firstly normalized the values in each season to the corresponding 2013 values and plotted the relative changes from the 2013 EPA point of each season to make the GOME-2B relative variations comparable to the other datasets. Shading in a lighter color is added to show the standard deviation of the results; when uncertainty is small due in part to a large number of data points, shading area may not show up.

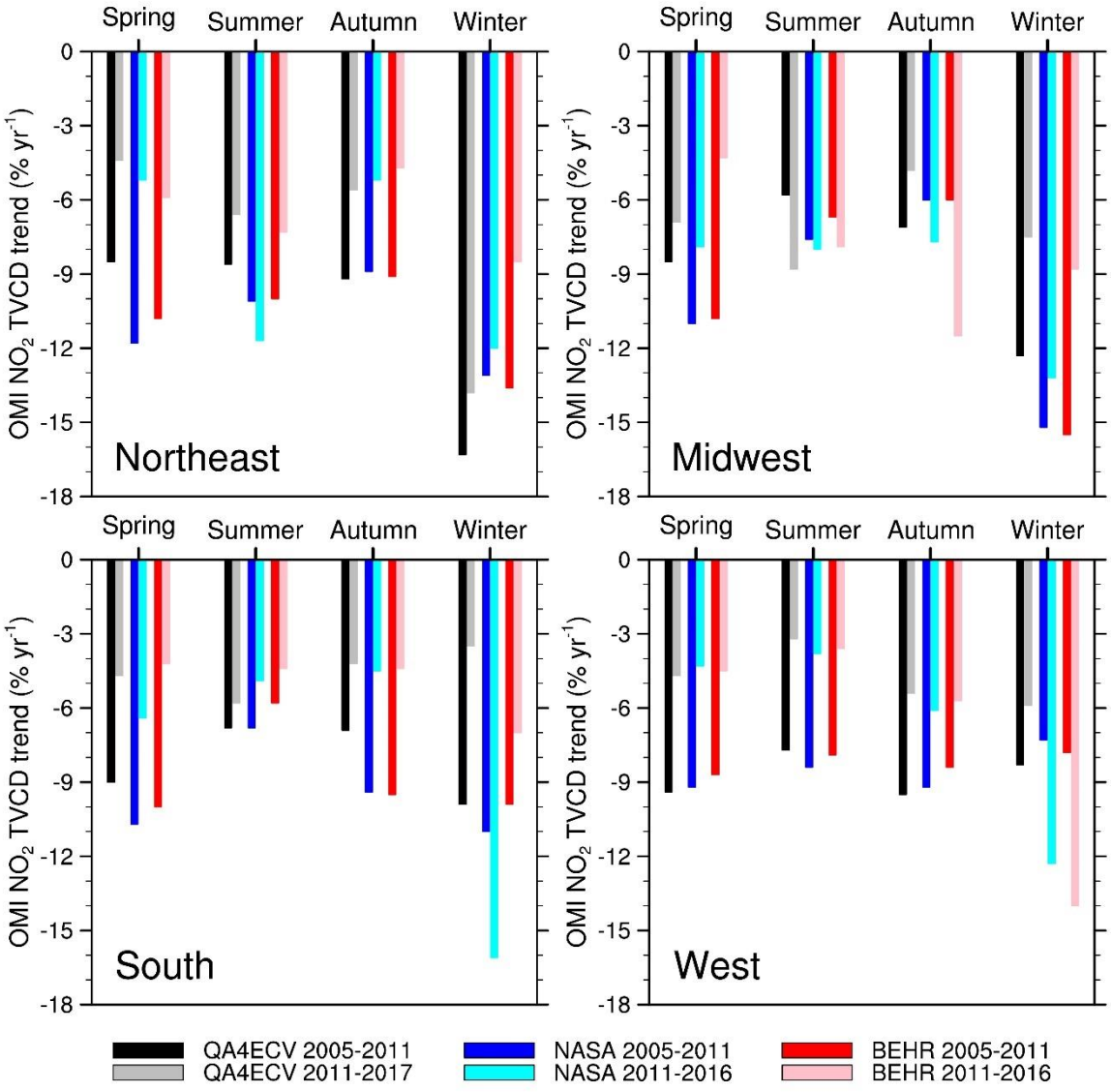

Figure 7. Pre- and post-2011 OMI NO_2 TVCD trends for 4 seasons in the urban regions of Northeast, Midwest, South, and West. Black bars denote OMI-QA4ECV NO_2 TVCD trends from 2005 – 2011; gray bars denote the corresponding trends during 2011 – 2017. Blue bars denote OMI-NASA trends from 2005 – 2011; cyan bars denote NASA-OMI trends from 2011 – 2016. Red bars denote BEHR-OMI trends from 2005 – 2011; pink bars denote OMI-BEHR trends from 2011 – 2016.

SUPPORTING INFORMATION AVAILABLE

Inferring the anthropogenic NO_x emission trend over the United States during 2003 - 2017 from satellite observations: Was there a flattening of the emission trend after the Great Recession?

Jianfeng Li[1], Yuhang Wang[1*]

[1]School of Earth and Atmospheric Sciences, Georgia Institute of Technology, Atlanta, Georgia, USA

[*] *Correspondence to* Yuhang Wang (yuhang.wang@eas.gatech.edu)

Figure Captions

Figure S1. Annual variation of NO_3^- wet deposition fluxes for each season from 2003 – 2017. The fluxes were scaled by the corresponding values in 2003. Shaded regions denote standard deviations. Monthly NO_3^- wet deposition observations are obtained from https://nadp.slh.wisc.edu/data/NTN/ntnAllsites.aspx (last access, September 29, 2019).

Figure S2~~1~~. Comparison between original EPA anthropogenic NO_x emissions and updated EPA anthropogenic NO_x emissions with the newest Continuous Emission Monitoring Systems (CEMS) measurements.

Figure S3~~2~~. Daily OMI NO_2 TVCDs for July 2011 (a) and 2012 (b) in Atlanta (33.755° N, 84.39° W). Black circles are weekday values, and red circles are weekend values. We find significant daily variations of NO_2 TVCD from (a) and (b). The number of available measurements in July 2011 is much less than July 2012. We find clear larger NO_2 TVCD values on weekdays than on weekends in July 2011, but the difference between weekday and weekday TVCDs in July 2012 are not so obvious.

Figure S4~~3~~. Hourly averaged ratios of FEM (a) and CAPS (b) to FRM NO_2 measurements in each season, respectively. The FEM/FRM ratios are computed from coincident FRM and FEM measurements from 2013 – 2015 at 4 sites. The CAPS/FRM ratios are calculated based on coincident CAPS and FRM data from 2015 – 2016 at 3 sites.

Figure S5~~4~~. Annual variations of AQS NO_2 surface concentrations at different hours on weekdays in spring (a, b), summer (c, d), autumn (e, f), and winter (g, h). Left panels show absolute NO_2 concentrations, and right panels are their relative variations normalized to 2011. To conduct reliable and consistent comparisons, we only used monitoring sites satisfying the seasonal *RCI* < 50% and continuity criteria on weekdays from 2003 – 2017.

Figure S6. Distributions of (a) NO_2 TVCD fraction that is in the boundary layer (< 2810 m) at 13:00 – 14:00, (b) NO_2 TVCD fraction in the boundary layer (< 1290 m) at 10:00 – 11:00, (c) the fraction of soil NO_x emissions in all surface sources (anthropogenic + soil) on weekdays for July 2011. As the lifetime of NO_2 in the free troposphere (several days ~ 2 weeks) is much longer than that in the boundary layer (~ 10 hours), local lightning NO_x emissions cannot represent NO_2 VCDs in the free troposphere. In this study, we apply NO_2 VCD in the free troposphere to analyze the impact of lighting NO_x on the nonlinear relationships between anthropogenic NO_x emissions and NO_2 TVCDs and use lightning NO_x and NO_2 VCD in the free troposphere interchangeably in the following.

Figure S7. (a) Distributions of the fractions of surface NO_x emissions emitted by soil ("SoilNO_x"), the portions of NO_2 TVCDs in the boundary layer ("PBLVCD"), and the fractions of NO_2 TVCDs from anthropogenic NO_x emissions ("AnthroVCD") as functions of NEI2011 anthropogenic NO_x emissions at 13:00 – 14:00 LT on weekdays for July 2011 over the CONUS. The fraction of NO_2 TVCDs from anthropogenic NO_x emissions is equal to $\left(1 - \frac{E_{soil}}{E_{soil}+E_{anthropogenic}}\right) \times \left(\frac{TVCD_{boundary}}{TVCD_{boundary}+TVCD_{free}}\right)$, where E_{soil} denotes soil NO_x emissions, $E_{anthropogenic}$ denotes anthropogenic NO_x emissions, $TVCD_{boundary}$ denotes NO_2 TVCDs in the boundary layer, and $TVCD_{free}$ denotes NO_2 TVCDs in the free troposphere. The calculated data are grouped into 9 bins as in Figure 2. (b) Same as (a), but for 10:00 – 11:00 LT. (c) Distributions of β_{Emis}, γ_{Emis}, β, and γ as functions of anthropogenic NO_x emissions at 13:00 – 14:00 LT on weekdays for July 2011 over the CONUS. β and γ are the same as Figure 2. β_{Emis} and γ_{Emis} denote β and γ values when no other factors are taken into consideration except for soil NO_x emissions, anthropogenic NO_x emissions, and NO_2 in the free troposphere. $\beta_{Emis} = \frac{15\%}{15\% \times \left(\frac{E_{anthropogenic}}{E_{anthropogenic}+E_{soil}}\right)\left(\frac{TVCD_{boundary}}{TVCD_{boudnary}+TVCD_{free}}\right)} = \left(\frac{E_{anthropogenic}+E_{soil}}{E_{anthropogenic}}\right)\left(\frac{TVCD_{boundary}+TVCD_{free}}{TVCD_{boundary}}\right)$,

and $\gamma_{Emis} = \frac{15\%}{15\% \times \left(\frac{E_{anthropogenic}}{E_{anthropogenic}+E_{soil}}\right)} = \left(\frac{E_{anthropogenic}+E_{soil}}{E_{anthropogenic}}\right)$. It is noteworthy that here we assume no interactions between the boundary layer and the free troposphere, boundary NO_x are only related to soil and anthropogenic NO_x emissions, and lightning NO_x only affect NO_2 in the free troposphere. The assumptions are reasonable as the time scale (~ 1 week) of the interactions between the boundary layer and the free troposphere are much longer than NO_x lifetime in the boundary layer, and in this study, only a small fraction of lightning NO_x is distributed into the boundary layer. Therefore, β_{Emis} and γ_{Emis} roughly represent the contributions of background sources (lightning NO_x and soil NO_x) to β and γ values. The differences between β (γ) and β_{Emis} (γ_{Emis}) indicate the contribution of non-emission factors to β (γ) values, such as chemistry, transport, and dry and wet depositions. (d) Same as (c), but for 10:00 – 11:00 LT. From this figure, we find that both background sources (lightning NO_x + soil NO_x) and non-emission factors are important when considering the nonlinear relationships among NO_x emissions, NO_2 surface concentrations, and NO_2 TVCDs in low-anthropogenic-NO_x emission regions.

Figure S8~~7~~. Same as Figure 4, but for AQS NO_2 surface concentrations and coincident GOME-2A NO_2 TVCD data during 2008 – 2016.

Figure S9~~8~~. Relative variations of OMI-QA4ECV NO_2 TVCD data for urban regions (black lines) and the whole CONUS (red lines) from 2005 – 2017 in 4 seasons.

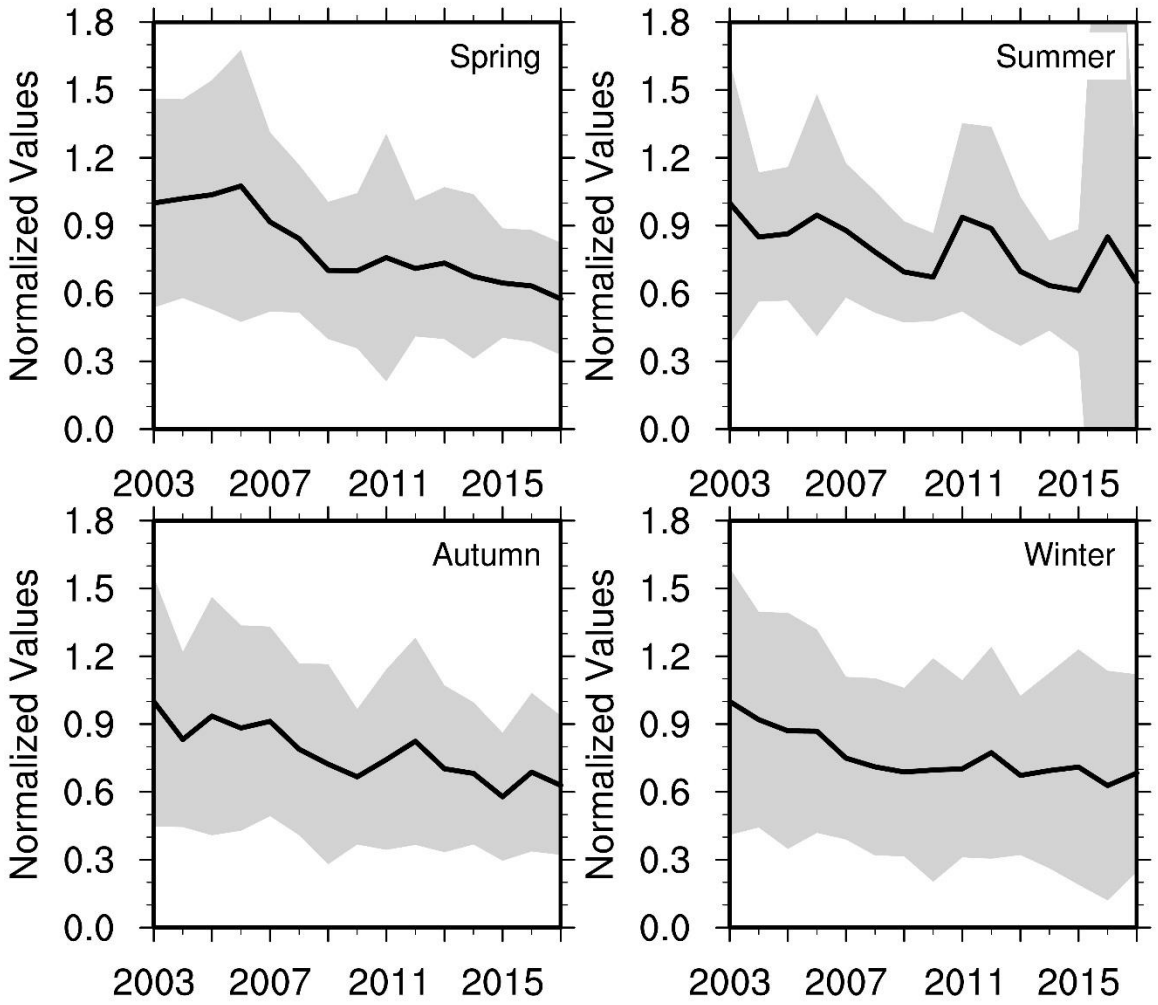

Figure S1. Annual variation of NO_3^- wet deposition fluxes for each season from 2003 – 2017. The fluxes were scaled by the corresponding values in 2003. Shaded regions denote standard deviations. Monthly NO_3^- wet deposition observations are obtained from https://nadp.slh.wisc.edu/data/NTN/ntnAllsites.aspx (last access, September 29, 2019).

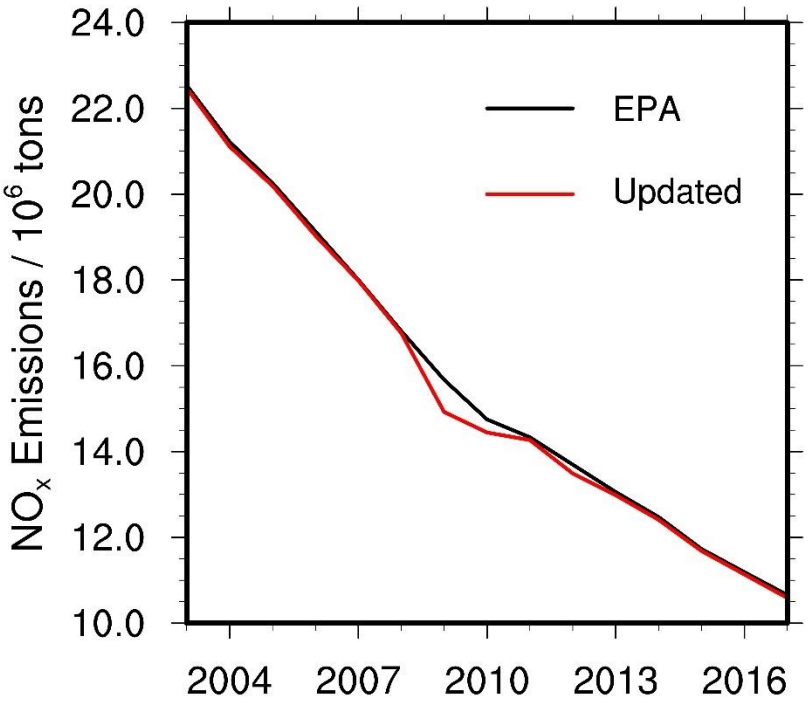

Figure S2~~1~~. Comparison between original EPA anthropogenic NO_x emissions and updated EPA anthropogenic NO_x emissions with the newest Continuous Emission Monitoring Systems (CEMS) measurements.

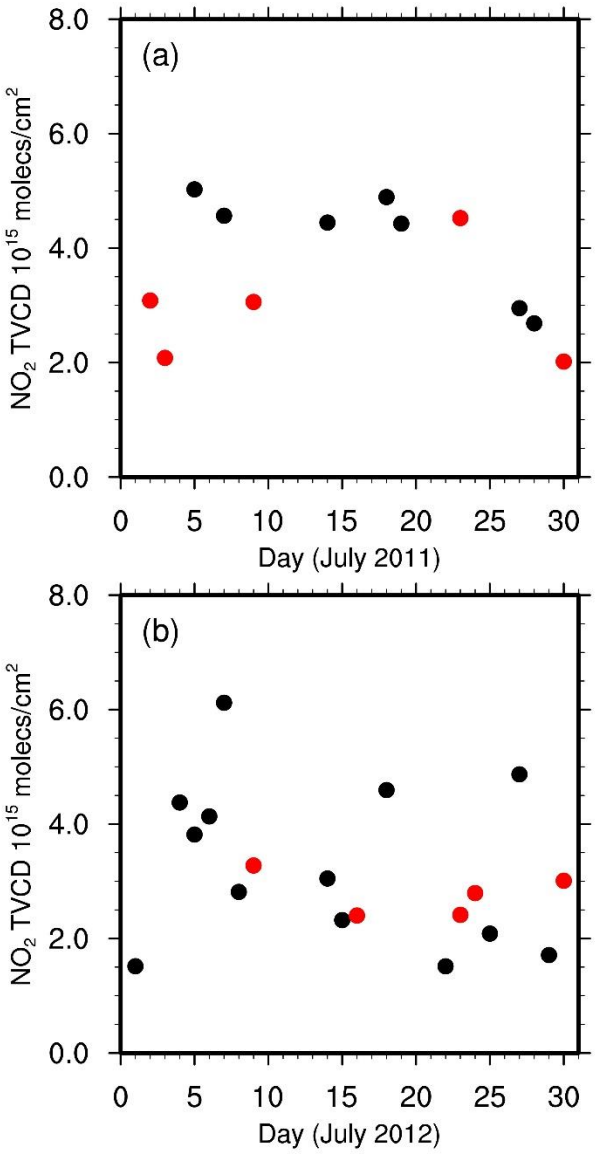

Figure S3~~2~~. Daily OMI NO_2 TVCDs for July 2011 (a) and 2012 (b) in Atlanta (33.755° N, 84.39° W). Black circles are weekday values, and red circles are weekend values. We find significant daily variations of NO_2 TVCD from (a) and (b). The number of available measurements in July 2011 is much less than July 2012. We find clear larger NO_2 TVCD values on weekdays than on weekends in July 2011, but the difference between weekday and weekday TVCDs in July 2012 are not so obvious.

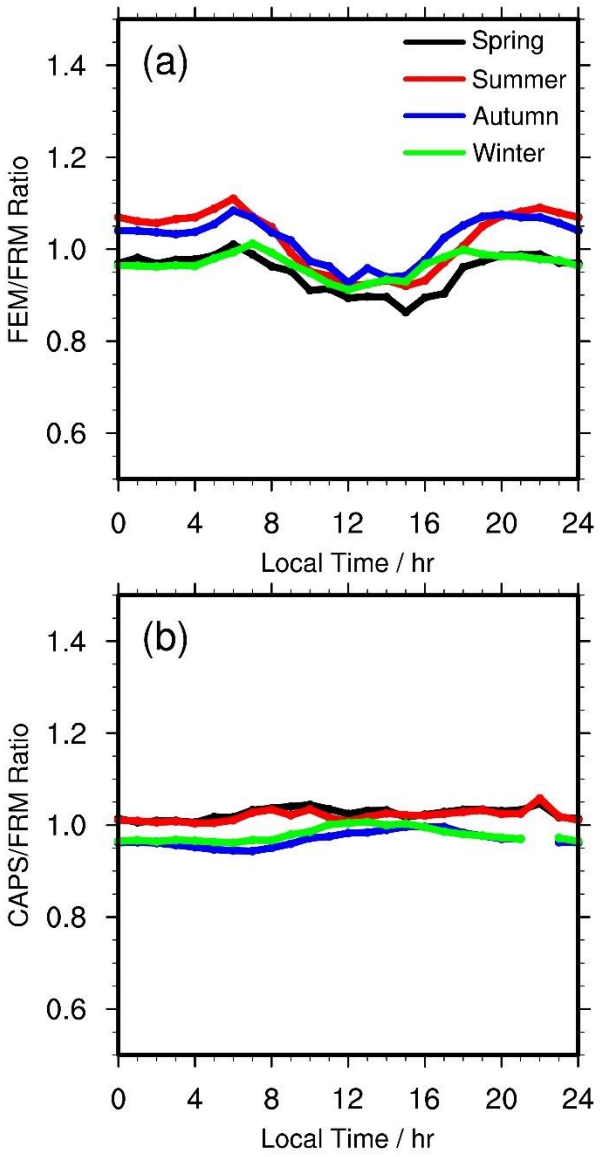

93

94 Figure S4~~3~~. Hourly averaged ratios of FEM (a) and CAPS (b) to FRM NO_2 measurements in each
95 season, respectively. The FEM/FRM ratios are computed from coincident FRM and FEM
96 measurements from 2013 – 2015 at 4 sites. The CAPS/FRM ratios are calculated based on
97 coincident CAPS and FRM data from 2015 – 2016 at 3 sites.

98

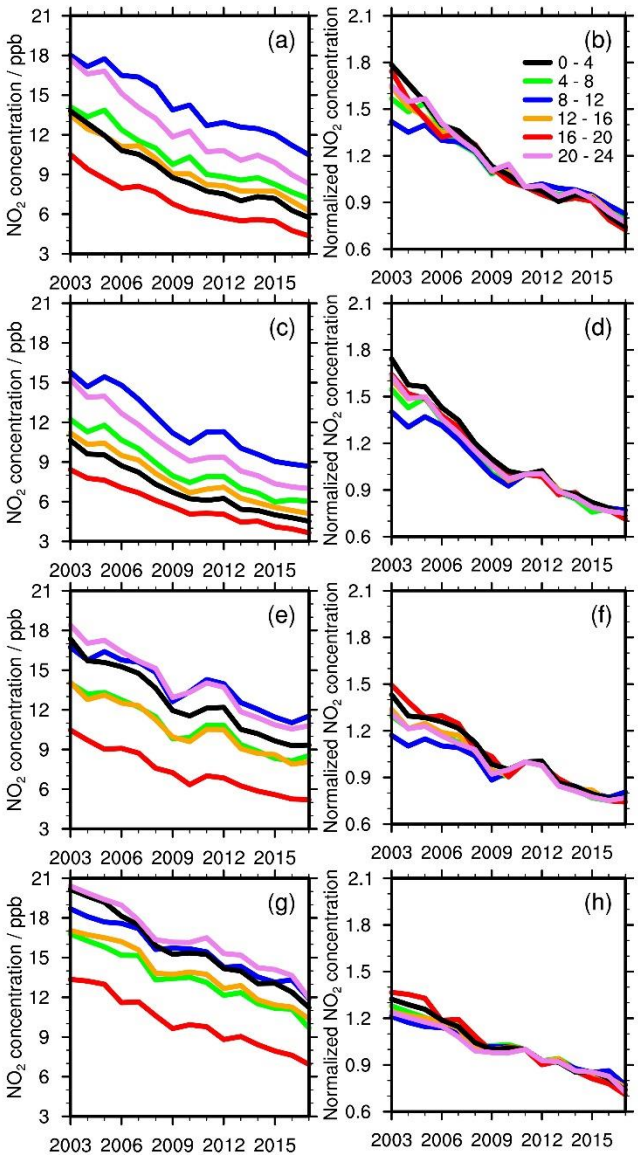

Figure S54. Annual variations of AQS NO_2 surface concentrations at different hours on weekdays in spring (a, b), summer (c, d), autumn (e, f), and winter (g, h). Left panels show absolute NO_2 concentrations, and right panels are their relative variations normalized to 2011. To conduct reliable and consistent comparisons, we only used monitoring sites satisfying the seasonal *RCI* < 50% and continuity criteria on weekdays from 2003 – 2017.

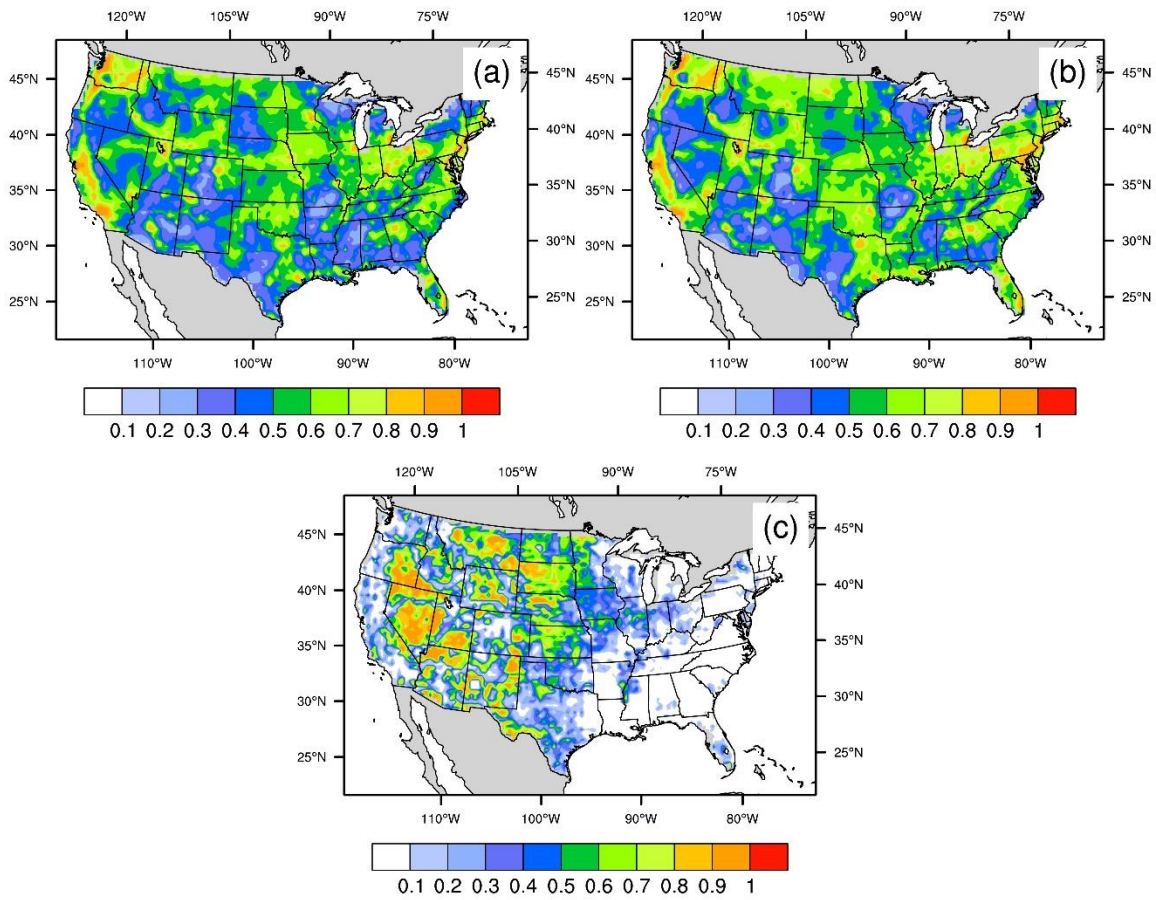

Figure S6. Distributions of (a) NO_2 TVCD fraction that is in the boundary layer (< 2810 m) at 13:00 – 14:00, (b) NO_2 TVCD fraction in the boundary layer (< 1290 m) at 10:00 – 11:00, (c) the fraction of soil NO_x emissions in all surface sources (anthropogenic + soil) on weekdays for July 2011. As the lifetime of NO_2 in the free troposphere (several days ~ 2 weeks) is much longer than that in the boundary layer (~ 10 hours), local lightning NO_x emissions cannot represent NO_2 VCDs in the free troposphere. In this study, we apply NO_2 VCD in the free troposphere to analyze the impact of lighting NO_x on the nonlinear relationships between anthropogenic NO_x emissions and NO_2 TVCDs and use lightning NO_x and NO_2 VCD in the free troposphere interchangeably in the following.

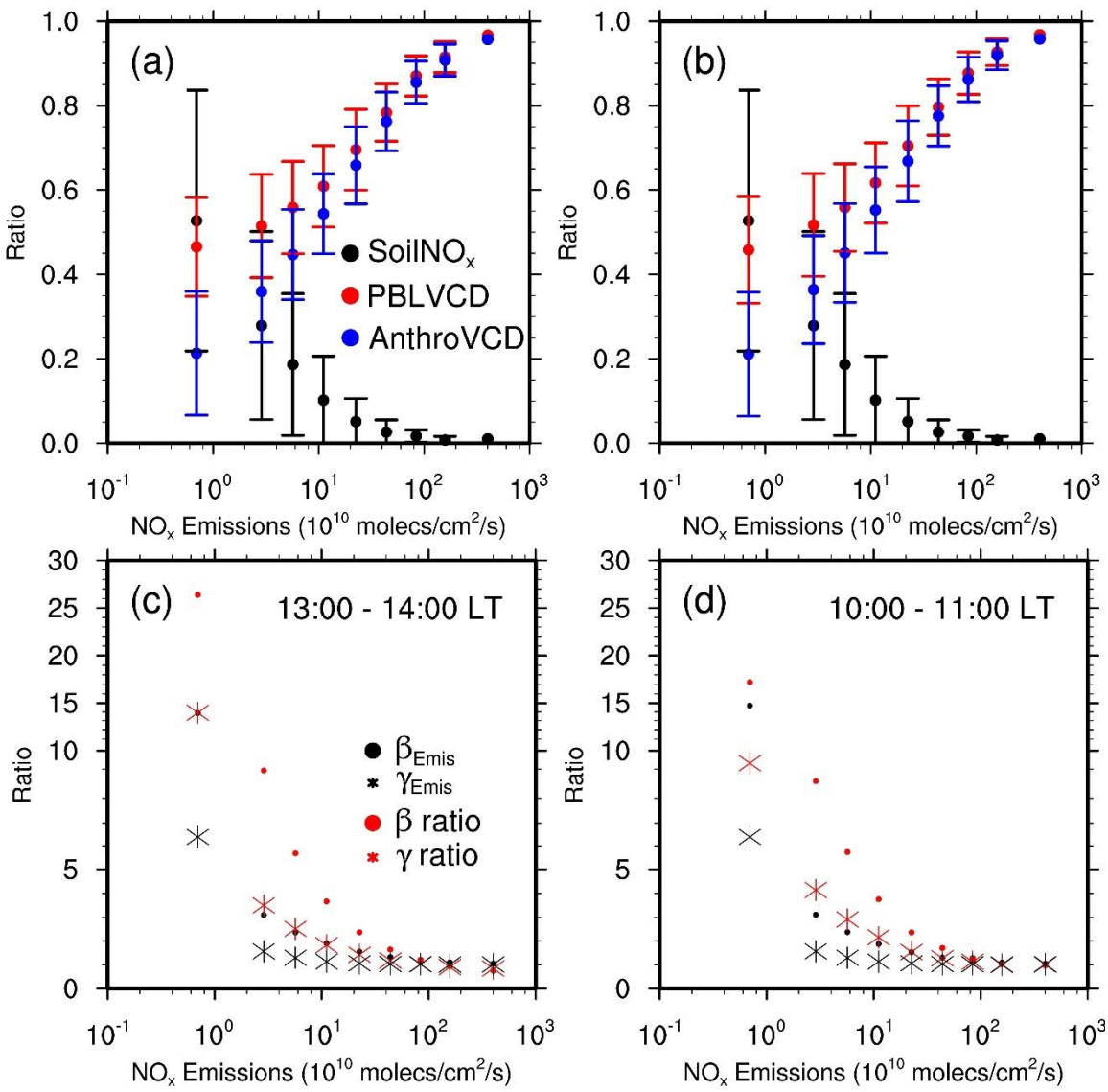

Figure S7. (a) Distributions of the fractions of surface NO_x emissions emitted by soil ("SoilNO_x"), the portions of NO_2 TVCDs in the boundary layer ("PBLVCD"), and the fractions of NO_2 TVCDs from anthropogenic NO_x emissions ("AnthroVCD") as functions of NEI2011 anthropogenic NO_x emissions at 13:00 – 14:00 LT on weekdays for July 2011 over the CONUS. The fraction of NO_2 TVCDs from anthropogenic NO_x emissions is equal to $\left(1 - \frac{E_{soil}}{E_{soil}+E_{anthropogenic}}\right) \times \left(\frac{TVCD_{boundary}}{TVCD_{boundary}+TVCD_{free}}\right)$, where E_{soil} denotes soil NO_x emissions,

$E_{anthropogenic}$ denotes anthropogenic NO_x emissions, $TVCD_{boundary}$ denotes NO_2 TVCDs in the boundary layer, and $TVCD_{free}$ denotes NO_2 TVCDs in the free troposphere. The calculated data are grouped into 9 bins as in Figure 2. (b) Same as (a), but for 10:00 – 11:00 LT. (c) Distributions of β_{Emis}, γ_{Emis}, β, and γ as functions of anthropogenic NO_x emissions at 13:00 – 14:00 LT on weekdays for July 2011 over the CONUS. β and γ are the same as Figure 2. β_{Emis} and γ_{Emis} denote β and γ values when no other factors are taken into consideration except for soil NO_x emissions, anthropogenic NO_x emissions, and NO_2 in the free troposphere. $\beta_{Emis} = \frac{15\%}{15\%\times\left(\frac{E_{anthropogenic}}{E_{anthropogenic}+E_{soil}}\right)\left(\frac{TVCD_{boundary}}{TVCD_{boudnary}+TVCD_{free}}\right)} = \left(\frac{E_{anthropogenic}+E_{soil}}{E_{anthropogenic}}\right)\left(\frac{TVCD_{boundary}+TVCD_{free}}{TVCD_{boundary}}\right)$, and $\gamma_{Emis} = \frac{15\%}{15\%\times\left(\frac{E_{anthropogenic}}{E_{anthropogenic}+E_{soil}}\right)} = \left(\frac{E_{anthropogenic}+E_{soil}}{E_{anthropogenic}}\right)$. It is noteworthy that here we assume no interactions between the boundary layer and the free troposphere, boundary NO_x are only related to soil and anthropogenic NO_x emissions, and lightning NO_x only affect NO_2 in the free troposphere. The assumptions are reasonable as the time scale (~ 1 week) of the interactions between the boundary layer and the free troposphere are much longer than NO_x lifetime in the boundary layer, and in this study, only a small fraction of lightning NO_x is distributed into the boundary layer. Therefore, β_{Emis} and γ_{Emis} roughly represent the contributions of background sources (lightning NO_x and soil NO_x) to β and γ values. The differences between β (γ) and β_{Emis} (γ_{Emis}) indicate the contribution of non-emission factors to β (γ) values, such as chemistry, transport, and dry and wet depositions. (d) Same as (c), but for 10:00 – 11:00 LT. From this figure, we find that both background sources (lightning NO_x + soil NO_x) and non-emission factors are important when considering the nonlinear relationships among NO_x emissions, NO_2 surface concentrations, and NO_2 TVCDs in low-anthropogenic-NO_x emission regions.

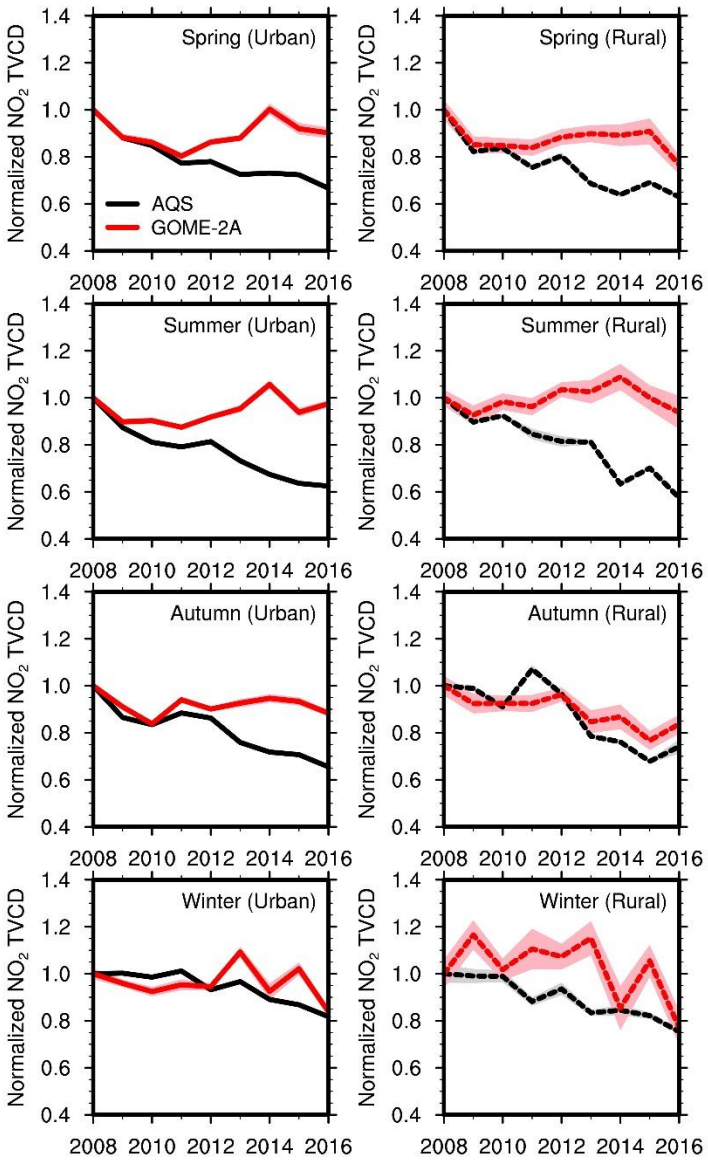

145

146 Figure S~~8~~5. Same as Figure 4, but for AQS NO_2 surface concentrations and coincident GOME-

147 2A NO_2 TVCD data during 2008 – 2016.

148

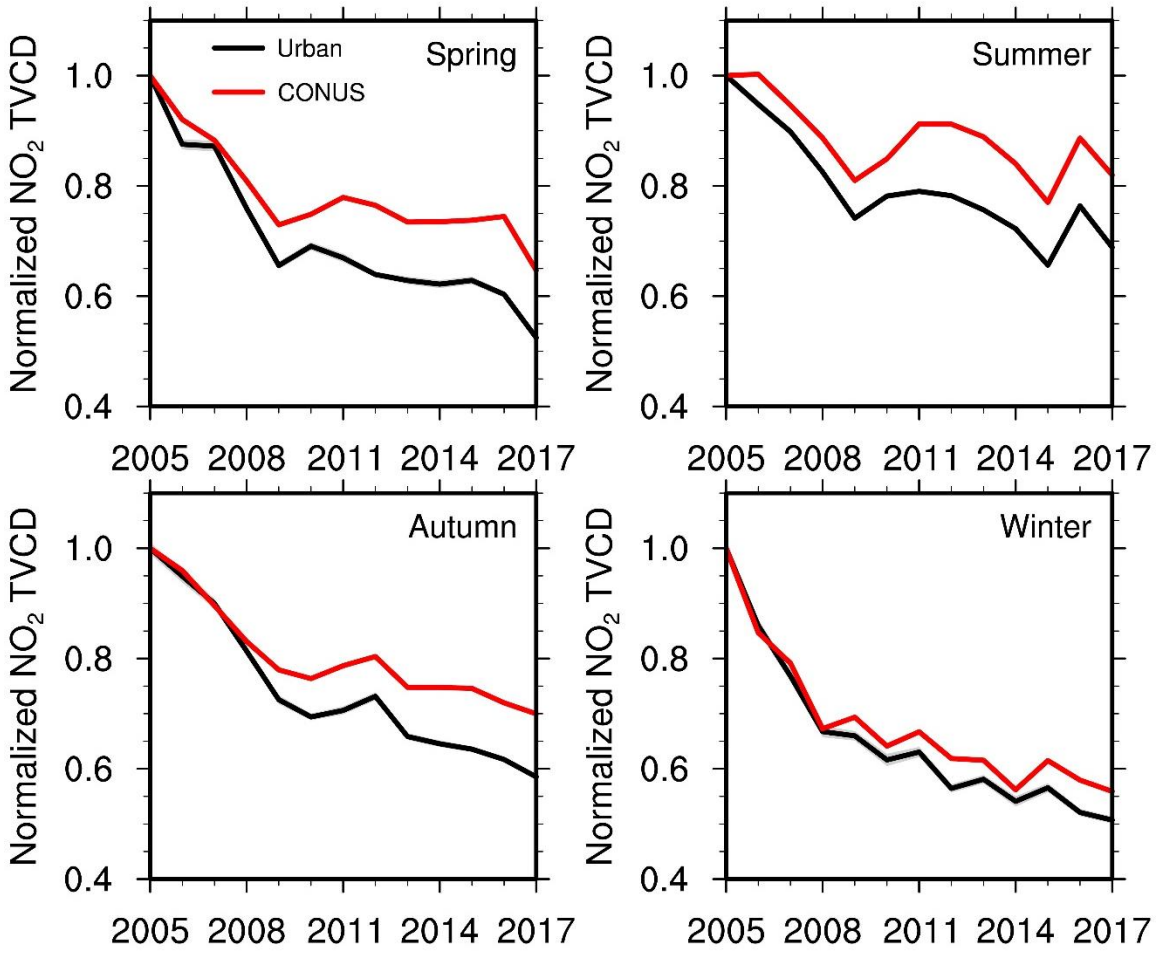

Figure S~~9~~6. Relative variations of OMI-QA4ECV NO_2 TVCD data for urban regions (black lines) and the whole CONUS (red lines) from 2005 – 2017 in 4 seasons.

SUPPORTING INFORMATION AVAILABLE

Inferring the anthropogenic NO_x emission trend over the United States during 2003 - 2017 from satellite observations: Was there a flattening of the emission trend after the Great Recession?

Jianfeng Li[1], Yuhang Wang[1*]

[1]School of Earth and Atmospheric Sciences, Georgia Institute of Technology, Atlanta, Georgia, USA

[*] *Correspondence to* Yuhang Wang (yuhang.wang@eas.gatech.edu)

Table Captions

Table S1. Summary of major satellite instruments for remote sensing of atmospheric NO_2 VCD in the past decade

Table S2. Summary of satellite NO_2 TVCD products and their retrieval information

Table S3. Selection criteria for satellite NO_2 TVCD pixel data

Table S4. Summary of annual trends of AQS NO_2 surface concentrations and satellite NO_2 TVCD products in each region during different periods

Table S1. Summary of major satellite instruments for remote sensing of atmospheric NO_2 VCD in the past decade

Instrument	Satellite	Launch date	End date	Operator	Equator crossing time (local time)	UV/Vis Spectral range (nm)	Spectral resolution (nm)	Swath length (km)	Nadir pixel resolution (km × km)	Global coverage (days)
SCIAMACHY	ENVISAT[1]	03/01/2002[2]	04/08/2012[2]	ESA[3]	10:00[1]	240 – 805[4]	0.24 – 0.48[4]	960[5]	60 × 30[5]	6[5]
GOME-2A	MetOp-A[6]	10/19/2006[6]	in operation	EUMETSAT[7]	9:30[8]	240 – 790[8]	0.26 – 0.51[8]	1920 before Jul. 15th, 2013; 960 after Jul. 15th, 2013[8]	80 × 40 before Jul. 15th, 2013; 40 × 40 after Jul. 15th, 2013[8]	1.5[9]
GOME-2B	MetOp-B[6]	09/17/2012[6]	In operation	EUMETSAT	9:30[8]	240 – 790[8]	0.26 – 0.51[8]	1920[8]	80 × 40[8]	1.5[9]
OMI	EOS-Aura[10]	07/152004[10]	In operation	NASA	13:45[10]	270 – 500[11]	0.45 – 1.0[11]	2600[11]	24 × 13[11]	1[11]

[1] Refer to https://earth.esa.int/web/guest/missions/esa-operational-eo-missions/envisat
[2] Refer to https://en.wikipedia.org/wiki/Envisat
[3] The European Space Agency
[4] Refer to http://www.iup.uni-bremen.de/sciamachy/instrument/performance/index.html
[5] Refer to Boersma et al. (2008), Boersma et al. (2009), and (Lee et al., 2009)
[6] Refer to https://www.eumetsat.int/website/home/Satellites/CurrentSatellites/Metop/index.html
[7] The European Organization for the Exploitation of Meteorological Satellites
[8] Refer to EUMETSAT (2015)
[9] Refer to Lee et al. (2009) and Wang et al. (2017)
[10] Refer to https://aura.gsfc.nasa.gov/
[11] Refer to https://aura.gsfc.nasa.gov/omi.html

Table S2. Summary of satellite NO_2 TVCD products and their retrieval information

NO_2 TVCD products	Version	Available period	DOAS fitting method	Stratosphere–troposphere separation	Fitting window (nm)	Albedo / reflectance	A priori profiles	Radiative transfer model	Cloud	Uncertainty
GOME-2B	TM4NO2A (2.3)	12/20/2012 – current	Intensity fit[1]	Assimilation of satellite total slant columns in the TM4 model[2, 3]	405 – 465[1]	Climatology albedo from 3 years of OMI data[4]	TM4 (2° × 3°)[2]	DAK[2]	FRESCO+ (Oxygen A-band around 760 nm)[5]	1.0×10^{15} molecules/cm^2 + 25%[2]
SCIAMACHY	QA4ECV (v1.1)	08/02/2002 – 04/08/2012	Optical Density[1, 6]	Assimilation of OMI total slant columns in the TM5 - MP model[6, 7]	425 – 465[6]	Climatology albedo based on SCIAMACHY[8]	TM5-MP (1° × 1°)[6]	DAK	FRESCO+	35% - 45% over polluted scenes; > 100% over background regions (Pacific Ocean)[6]
GOME-2A	QA4ECV (v1.1)	02/01/2007 – 12/31/2016			405 – 465[1, 6]	Climatology albedo based on GOME-2A[8]			FRESCO+	
OMI-QA4ECV	QA4ECV (v1.1)	10/012004 – Current			405 – 465[1, 6]	Climatology albedo from 5 years of OMI data[6]			Improved O_2-O_2 (477 nm)[9]	
OMI-NASA	SPv3	01/01/2005 – 07/31/2017	Stepwise intensity fit with monthly averaged solar irradiance spectrum[1, 10]	Based on OMI total slant columns over regions with low estimated TVCD contributions (TVCD contributions less than 0.3×10^{15} molecules/cm^2)[10]	402 – 465[1, 10]	OMI climatology albedo[10]	GMI (1° × 1.25°)[10]	TMORAD[10]	O_2-O_2 (477 nm)[10, 11]	SPv2.1 TVCD has uncertainties of about 30% under clear-sky conditions to about 60% under cloudy conditions[12], and the relative difference between SPv3 and SPv2.1 is less than ~20%[10].
OMI-BEHR[13]	v3.0B	01/01/2005 – 07/31/2017				Based on MCD43D BRDF product (for land) and model parameterization (for ocean)	WRF-Chem (12 km)			~ 45% on average[14]

[1] Refer to Zara et al. (2018)
[2] Refer to Boersma et al. (2011). "TM4" is the Tracer Model, version 4. "DAK" is the Doubling-Adding KNMI (DAK) radiative transfer model.
[3] Refer to Williams et al. (2009)
[4] Refer to Kleipool et al. (2008)
[5] Refer to Wang et al. (2017) and Wang et al. (2008)
[6] Refer to Boersma et al. (2018)
[7] Refer to Williams et al. (2017)
[8] Refer to Tilstra et al. (2017)
[9] Refer to Veefkind et al. (2016)
[10] Refer to Bucsela et al. (2013), Bucsela et al. (2016), Krotkov et al. (2017), and Marchenko et al. (2015). "TMORAD" is the TMOS radiative transfer model.
[11] Refer to Acarreta et al. (2004)
[12] Refer to Lamsal et al. (2014), Oetjen et al. (2013), and Tong et al. (2015)
[13] Refer to Laughner et al. (2018). OMI-BEHR uses the SCD from OMI-NASA SPv3 but updates inputs for the AMF calculation, such as a prior NO_2 vertical profiles and surface reflectance. Besides, OMI-BEHR only provides NO_2 TVCD over the contiguous United States (CONUS). As in this study, we used the OMI-NASA datasets archived in the OMI-BEHR product, so we only obtained OMI-NASA datasets extended to July 31, 2017.
[14] Average uncertainty over the CONUS is calculated based on the file from http://behr.cchem.berkeley.edu/behr/BEHR-us-uncertainty.hdf

Table S3. Selection criteria for satellite NO_2 TVCD pixel data

NO_2 TVCD products	Period	Solar zenith angle	albedo	Cloud radiance fraction	Snow or ice covered	AMFtrop/AMFgeo	Flag for retrieval success	Retrieval quality flag	Rows in swath
GOME-2B	01/01/2013 – 12/31/2017	< 80°	<= 0.3	<= 50%	No	> 0.2	Yes		All
SCIAMACHY	01/01/2003 – 12/31/2011	< 80°	<= 0.3	<= 50%	No	> 0.2	Yes		All
GOME-2A	01/01/2008 – 12/31/2016	< 80°	<= 0.3	<= 50%	No	> 0.2	Yes		All
OMI-QA4ECV[1]	01/01/2005 – 12/31/2017	< 80°	<= 0.3	<= 50%	No	> 0.2	Yes		6 - 21
OMI-NASA[1]	01/01/2005 – 12/31/2016	< 80°	<= 0.3	<= 50%			Yes	Yes	6 – 21
OMI-BEHR[1]	01/01/2005 – 12/31/2016	< 80°	<= 0.3	<= 50%			Yes	Yes	6 - 21

[1] Rows 6-21 are selected to remove the anomalies developed in the OMI sensor (Boersma et al., 2018; Zhang et al., 2018).

Table S4. Summary of annual trends of AQS NO_2 surface concentrations and satellite NO_2 TVCD products in each region during different periods[1]

		Northeast		Midwest		South		West	
		AQS site	CONUS	AQS site	CONUS	AQS site	CONUS	AQS site	CONUS
AQS NO_2 VMR at 13:00 -14:00	2003 – 2011	-6.8 ± 0.7%		-6.1 ± 1.2%		-6.6 ± 0.7%		-7.6 ± 1.2%	
	2011 – 2017	-8.0 ± 1.2%		-6.4 ± 0.8%		-5.8 ± 0.6%		-7.2 ± 1.6%	
AQS NO_2 VMR at 10:00 – 11:00	2003 – 2011	-6.6 ± 0.5%		-5.8 ± 1.5%		-6.5 ± 1.3%		-7.1 ± 1.6%	
	2011 – 2017	-7.6 ± 1.0%		-6.8 ± 0.5%		-5.7 ± 0.1%		-6.1 ± 1.1%	
SCIAMACHY	2003 – 2011	-17.1 ± 2.7%	-11.0 ± 3.3%	-12.9 ± 6.8%	-6.5 ± 0.8%	-9.1 ± 1.0%	-6.2 ± 1.5%	-9.1 ± 1.8%	-7.0 ± 1.4%
	2011 – 2017								
GOME2B	2003 – 2011								
	2013 – 2017	-11.4 ± 3.7%	-10.8 ± 3.9%	-9.9 ± 13.1%	-4.4 ± 27.2%	-8.9 ± 3.0%	-7.5 ± 3.6%	-11.8 ± 3.0%	-10.6 ± 2.3%
OMI-QA4ECV	2005 – 2011	-14.2 ± 6.3%	-10.6 ± 3.8%	-9.2 ± 4.2%	-8.4 ± 2.8%	-9.2 ± 2.7%	-8.2 ± 1.5%	-10.5 ± 1.6%	-8.7 ± 0.9%
	2011 – 2017	-18.0 ± 16.2%	-7.6 ± 4.2%	-7.6 ± 3.3%	-7.0 ± 1.7%	-4.8 ± 1.4%	-4.6 ± 1.0%	-6.4 ± 1.4%	-4.8 ± 1.2%
OMI-NASA	2005 – 2011	-11.8 ± 1.3%	-11.0 ± 1.8%	-10.9 ± 4.8%	-10.0 ± 4.1%	-10.0 ± 3.5%	-9.5 ± 1.9%	-10.2 ± 1.8%	-8.5 ± 0.9%
	2011 – 2016	-10.0 ± 4.9%	-8.5 ± 3.8%	-13.2 ± 3.2%	-9.2 ± 2.7%	0.3 ± 19.2%	-8.0 ± 5.5%	-9.0 ± 5.7%	-6.6 ± 3.9%
OMI-BEHR	2005 – 2011	-11.8 ± 1.8%	-10.9 ± 1.9%	-12.2 ± 7.3%	-9.8 ± 4.4%	-9.5 ± 3.1%	-8.8 ± 2.0%	-9.9 ± 1.1%	-8.2 ± 0.4%
	2011 – 2016	-8.2 ± 3.4%	-6.6 ± 1.7%	-27.4 ± 24.3%	-8.1 ± 3.0%	-7.2 ± 2.3%	-5.0 ± 1.3%	-13.2 ± 14.5%	-7.0 ± 4.8%

[1] Annual trends are the averages of regional seasonal trends (e.g, Figure 7).

References

Acarreta, J. R., de Haan, J. F., and Stammes, P.: Cloud pressure retrieval using the O_2-O_2 absorption band at 477 nm, J. Geophys. Res.-Atmos., 109, 10.1029/2003JD003915, 2004.

Boersma, K. F., Jacob, D. J., Eskes, H. J., Pinder, R. W., Wang, J., and Van Der A, R. J.: Intercomparison of SCIAMACHY and OMI tropospheric NO_2 columns: Observing the diurnal evolution of chemistry and emissions from space, J. Geophys. Res.-Atmos., 113, 10.1029/2007JD008816, 2008.

Boersma, K. F., Jacob, D. J., Trainic, M., Rudich, Y., De Smedt, I., Dirksen, R., and Eskes, H. J.: Validation of urban NO_2 concentrations and their diurnal and seasonal variations observed from the SCIAMACHY and OMI sensors using in situ surface measurements in Israeli cities, Atmos. Chem. Phys., 9, 3867-3879, 10.5194/acp-9-3867-2009, 2009.

Boersma, K. F., Eskes, H. J., Dirksen, R. J., Veefkind, J. P., Stammes, P., Huijnen, V., Kleipool, Q. L., Sneep, M., Claas, J., and Leitão, J.: An improved tropospheric NO_2 column retrieval algorithm for the Ozone Monitoring Instrument, Atmos. Meas. Tech., 4, 1905-1928, 10.5194/amt-4-1905-2011, 2011.

Boersma, K. F., Eskes, H. J., Richter, A., De Smedt, I., Lorente, A., Beirle, S., van Geffen, J. H., Zara, M., Peters, E., and Roozendael, M. V.: Improving algorithms and uncertainty estimates for satellite NO_2 retrievals: results from the quality assurance for the essential climate variables (QA4ECV) project, Atmos. Meas. Tech., 11, 6651-6678, 10.5194/amt-11-6651-2018, 2018.

Bucsela, E. J., Krotkov, N. A., Celarier, E. A., Lamsal, L. N., Swartz, W. H., Bhartia, P. K., Boersma, K. F., Veefkind, J. P., Gleason, J. F., and Pickering, K. E.: A new stratospheric and tropospheric NO_2 retrieval algorithm for nadir-viewing satellite instruments: applications to OMI, Atmos. Meas. Tech., 6, 2607-2626, 10.5194/amt-6-2607-2013, 2013.

Bucsela, E. J., Celarier, E. A., Gleason, J. L., Krotkov, N. A., Lamsal, L. N., Marchenko, S. V., and Swartz, W. H.: OMNO2 README Document Data Product Version 3.0, NASA, 38, 2016.

EUMETSAT: GOME_FACTSHEET, Germany, 33, 2015.

Kleipool, Q. L., Dobber, M. R., de Haan, J. F., and Levelt, P. F.: Earth surface reflectance climatology from 3 years of OMI data, J. Geophys. Res.-Atmos., 113, 10.1029/2008JD010290, 2008.

Krotkov, N. A., Lamsal, L. N., Celarier, E. A., Swartz, W. H., Marchenko, S. V., Bucsela, E. J., Chan, K. L., Wenig, M., and Zara, M.: The version 3 OMI NO_2 standard product, Atmos. Meas. Tech., 10, 3133-3149, 10.5194/amt-10-3133-2017, 2017.

Lamsal, L. N., Krotkov, N. A., Celarier, E. A., Swartz, W. H., Pickering, K. E., Bucsela, E. J., Gleason, J. F., Martin, R. V., Philip, S., and Irie, H.: Evaluation of OMI operational standard NO_2 column retrievals using in situ and surface-based NO_2 observations, Atmos. Chem. Phys., 14, 11587-11609, 10.5194/acp-14-11587-2014, 2014.

Laughner, J. L., Zhu, Q., and Cohen, R. C.: The Berkeley High Resolution Tropospheric NO_2 product, Earth System Science Data, 10, 2069-2095, 10.5194/essd-10-2069-2018, 2018.

Lee, C., Martin, R. V., van Donkelaar, A., Richter, A., Burrows, J. P., and Kim, Y. J.: Remote Sensing of Tropospheric Trace Gases (NO_2 and SO_2) from SCIAMACHY, in: Atmospheric and Biological Environmental Monitoring, Springer, 63-72, 2009.

Marchenko, S., Krotkov, N. A., Lamsal, L. N., Celarier, E. A., Swartz, W. H., and Bucsela, E. J.: Revising the slant column density retrieval of nitrogen dioxide observed by the Ozone Monitoring Instrument, J. Geophys. Res.-Atmos., 120, 5670-5692, 10.1002/2014JD022913, 2015.

Oetjen, H., Baidar, S., Krotkov, N. A., Lamsal, L. N., Lechner, M., and Volkamer, R.: Airborne MAX-DOAS measurements over California: Testing the NASA OMI tropospheric NO_2 product, J. Geophys. Res.-Atmos., 118, 7400-7413, 10.1002/jgrd.50550, 2013.

Tilstra, L. G., Tuinder, O. N. E., Wang, P., and Stammes, P.: Surface reflectivity climatologies from UV to NIR determined from Earth observations by GOME-2 and SCIAMACHY, J. Geophys. Res.-Atmos., 122, 4084-4111, 10.1002/2016JD025940, 2017.

Tong, D., Lamsal, L., Pan, L., Ding, C., Kim, H., Lee, P., Chai, T., Pickering, K. E., and Stajner, I.: Long-term NO_x trends over large cities in the United States during the great recession: Comparison of satellite retrievals, ground observations, and emission inventories, Atmos. Environ., 107, 70-84, 10.1016/j.atmosenv.2015.01.035, 2015.

Veefkind, J. P., de Haan, J. F., Sneep, M., and Levelt, P. F.: Improvements to the OMI O_2–O_2 operational cloud algorithm and comparisons with ground-based radar–lidar observations, Atmos. Meas. Tech., 9, 6035-6049, 10.5194/amt-9-6035-2016, 2016.

Wang, P., Stammes, P., van der A, R., Pinardi, G., and van Roozendael, M.: FRESCO+: an improved O_2 A-band cloud retrieval algorithm for tropospheric trace gas retrievals, Atmos. Chem. Phys., 8, 6565-6576, 10.5194/acp-8-6565-2008, 2008.

Wang, Y., Beirle, S., Lampel, J., Koukouli, M., De Smedt, I., Theys, N., Ang, L., Wu, D., Xie, P., and Liu, C.: Validation of OMI, GOME-2A and GOME-2B tropospheric NO_2, SO_2 and HCHO products using MAX-DOAS observations from 2011 to 2014 in Wuxi, China: investigation of the effects of priori profiles and aerosols on the satellite products, Atmos. Chem. Phys., 17, 5007, 10.5194/acp-17-5007-2017, 2017.

Williams, J. E., Scheele, M. P., van Velthoven, P. F. J., Cammas, J.-P., Thouret, V., Galy-Lacaux, C., and Volz-Thomas, A.: The influence of biogenic emissions from Africa on tropical tropospheric ozone during 2006: a global modeling study, Atmos. Chem. Phys., 9, 5729-5749, 10.5194/acp-9-5729-2009, 2009.

Williams, J. E., Boersma, K. F., Sager, P. L., and Verstraeten, W. W.: The high-resolution version of TM5-MP for optimized satellite retrievals: description and validation, Geoscientific Model Development, 10, 721-750, 10.5194/gmd-10-721-2017, 2017.

Zara, M., Boersma, K. F., De Smedt, I., Richter, A., Peters, E., Van Geffen, J. H. G. M., Beirle, S., Wagner, T., Van Roozendael, M., and Marchenko, S.: Improved slant column density retrieval

of nitrogen dioxide and formaldehyde for OMI and GOME-2A from QA4ECV: intercomparison, uncertainty characterization, and trends, Meas. Tech. Discuss, 1-47, 10.5194/amt-11-4033-2018, 2018.

Zhang, R., Wang, Y., Smeltzer, C., Qu, H., Koshak, W., and Boersma, K. F.: Comparing OMI-based and EPA AQS in situ NO_2 trends: towards understanding surface NO_x emission changes, Atmos. Meas. Tech., 11, 3955-3967, 10.5194/amt-11-3955-2018, 2018.